GSDMD-dependent platelet pyroptosis exacerbates NET formation and inflammation in severe sepsis

WaiHo Tang (waiho.tang@gwcmc.org)
Guangzhou Women and Children's Medical Center

Meiling Su
Institute of Pediatrics, Guangzhou Women and Children's Medical Centre

Chaofei Chen
Institute of Pediatrics, Guangzhou Women and Children's Medical Centre

Shaoying Li
Institute of Pediatrics, Guangzhou Women and Children's Medical Centre

Musheng Li
Institute of Pediatrics, Guangzhou Women and Children's Medical Centre

Zhi Zeng
Institute of Pediatrics, Guangzhou Women and Children's Medical Centre

Yuan Zhang
Institute of Pediatrics, Guangzhou Women and Children's Medical Centre

Luoxing Xia
Institute of Pediatrics, Guangzhou Women and Children's Medical Centre

Xiuzhen Li
Institute of Pediatrics, Guangzhou Women and Children's Medical Centre

Dezhong Zheng
Department of Cardiology, Third Affiliated Hospital of Southern Medical University

Qiqi Lin
Institute of Pediatrics, Guangzhou Women and Children's Medical Centre

Xuejiao Fan
Institute of Pediatrics, Guangzhou Women and Children's Medical Centre

Ying Wen
Institute of Pediatrics, Guangzhou Women and Children's Medical Centre

Yingying Liu
Institute of Pediatrics, Guangzhou Women and Children's Medical Centre

Feiyan Chen
Institute of Pediatrics, Guangzhou Women and Children's Medical Centre

Wei Luo
Institute of Pediatrics, Guangzhou Women and Children's Medical Centre

Yun Bu

Institute of Pediatrics, Guangzhou Women and Children's Medical Centre
Jinhong Qin
Institute of Pediatrics, Guangzhou Women and Children's Medical Centre
Manli Guo
Institute of Pediatrics, Guangzhou Women and Children's Medical Centre
Miaoyun Qiu
Guangzhou Women and Children's Medical Center
Lei Sun
Institute of Pediatrics, Guangzhou Women and Children's Medical Centre
Renjing Liu
Victor Chang Cardiac Research Institute
Ping Wang
Institute of Pediatrics, Guangzhou Women and Children's Medical Centre
John Hwa
Yale University https://orcid.org/0000-0001-7366-2628

Article

Keywords:

Posted Date: March 21st, 2022

DOI: https://doi.org/10.21203/rs.3.rs-1462784/v1

Version of Record: A version of this preprint was published at Nature Cardiovascular Research on August 4th, 2022. See the published version at https://doi.org/10.1038/s44161-022-00108-7.

GSDMD-dependent platelet pyroptosis exacerbates NET formation and inflammation in severe sepsis

Meiling Su[1#], Chaofei Chen[1, 3#], Shaoying Li[1], Musheng Li[1], Zhi Zeng[1], Yuan Zhang[1], Luoxing Xia[1], Xiuzhen Li[1], Dezhong Zheng[5], Qiqi Lin[1], Xuejiao Fan[1], Ying Wen[1], Yingying Liu[1], Feiyan Chen[1], Wei Luo[1], Yun Bu[1], Jinhong Qin[1], Manli Guo[1], Miaoyun Qiu[1], Lei Sun[1], Renjing Liu[4], Ping Wang[1]*, John Hwa[2]*, Wai Ho Tang[1,6]*

[1]Institute of Pediatrics, Guangzhou Women and Children's Medical Centre, Guangzhou Medical University, Guangzhou, 510080, China; [2]Section of Cardiovascular Medicine, Department of Internal Medicine, Yale Cardiovascular Research Center, Yale University School of Medicine, New Haven, 06511, CT, USA; [3]The Joint Center for Infection and Immunity, a. Guangzhou Institute of Pediatrics, Guangzhou Women and Children's Medical Center, Guangzhou, 510623, China；b. Institute Pasteur of Shanghai, Chinese Academy of Science, Shanghai, 200031, China；[4]Victor Chang Cardiac Research Institute, Sydney, Australia; [5]Department of Cardiology, Third Affiliated Hospital of Southern Medical University, Southern Medical University, 183 Zhongshan Avenue West, Guangzhou, 510630, China. [6]School of Nursing and Health Studies, Hong Kong Metropolitan University, Ho Man Tin, Kowloon, Hong Kong SAR, China.

[#]These authors contributed equally to this work.

John Hwa, MD, PhD
Yale Cardiovascular Research Center,
Section of Cardiovascular Medicine,
Department of Internal Medicine,
Yale University School of Medicine,
New Haven, 06511, CT, USA
Tel: 203-7375583
Email: john.hwa@yale.edu

Wai Ho Tang, PhD
Institute of Pediatrics,
Guangzhou Women and Children's Medical Centre,
Guangzhou Medical University,
Guangzhou, Guangdong, 510623, China
Tel: (+86) 020-38076327
Email: waiho.tang@gwcmc.org

*Address for Correspondence:

Conflict of interest: The authors declare that they have no competing interests.

Abstract

Dysregulated inflammation is closely associated with increased mortality in sepsis. Platelets have emerged as key inflammatory cells implicated in the pathology of sepsis, including the development of thrombosis, thrombocytopenia, and neutrophil extracellular traps (NETs). Platelet's contributions to rapid clinical deterioration and dysregulated inflammation in sepsis have not been defined. In our cohort, the incidence of thrombocytopenia, thrombocytopathy and excessive inflammatory cytokines released in patients with severe sepsis were significantly increased. Platelet proteomic analysis revealed significant up-regulation of Gasdermin D (GSDMD). Using platelet-specific *Gsdmd* deficient mice, we demonstrated a requirement for GSDMD in triggering platelet pyroptosis in cecal ligation and puncture (CLP)-induced sepsis. We further demonstrated that GSDMD-dependent platelet pyroptosis was induced by high levels of S100A8/A9 targeting platelet toll-like receptor 4 (TLR4). Pyroptotic platelet-derived oxidized mitochondrial DNA (ox-mtDNA) potentially promoted NET formation, which in turn contributed to platelet pyroptosis via the release of S100A8/A9, forming a positive feedback loop that led to excessive inflammatory cytokines release. Both pharmacological inhibition using Paquinimod and genetic ablation of the S100A8/A9-TLR4 signaling axis suppressed GSDMD-dependent platelet pyroptosis, thereby alleviating NET-mediated inflammation and improving survival in CLP-induced sepsis mice. Taken together, these findings provide new insights into the proinflammatory role of platelet pyroptosis in severe sepsis.

Introduction

Sepsis, the leading cause of morbidity, mortality, and healthcare utilization for children worldwide, is characterized by a dysregulated inflammatory response to infection[1]. The incidence of sepsis varies substantially across age, peaking in early childhood[2]. The development of inflammation-related thrombocytopathy during sepsis is recognized as a significant event associated with increased severity of sepsis, leading to higher mortality[3]. Platelets have emerged as key inflammatory cells implicated in the pathophysiology of sepsis[4], however, the role of platelets in exacerbating severe sepsis has not been clearly defined.

Pyroptosis, a form of inflammation or infection-induced cell death, is critical for immunity[5]. Pyroptosis plays a pivotal role in the defense against viral and microbial infections[6]. Platelets have the necessary components for pyroptosis including NOD-like receptors containing domain pyrin 3 (NLRP3) inflammasome, adaptor-apoptosis-associated speck-like protein (ASC), caspase 1 and IL-1β[7,8]. The NLRP3 inflammasome is implicated in sensing intracellular danger signals in innate immunity and pathogenic inflammation[9]. During pyroptosis, the activation of the NLRP3 inflammasome results in Gasdermin D (GSDMD)-pore formation, cell swelling, and a burst of inflammatory cytokines and cytosolic content release. Of note, mitochondria are a source of reactive oxygen species (ROS) and mitochondrial DNA (mtDNA), which have recently been implicated in inflammatory responses[10,11]. Oxidized mtDNA (ox-mtDNA) is pro-inflammatory, participating in

the formation of polymorphonuclear neutrophils (PMNs) extracellular traps (NETs) in autoimmune diseases[12]. NETs are described as a double-edged sword in innate immunity: NETs serve to defend against bacterial infection, while they produce proinflammatory molecules to amplify the inflammatory response[13]. However, there is no direct evidence that platelet pyroptosis occurs in sepsis, and if present, whether it participates in NET formation and immune host response in severe sepsis.

Previous studies have suggested that the abundance of S100A8/A9 (calprotectin, myeloid-related protein-8/14) protein was released from PMNs[14] and NETs[15] at the site of inflammation. Heterodimer S100A8/A9 is an alarmin damage associated molecular pattern that is rapidly released from myeloid lineage cells upon stress or cell/tissue damage, acting as a secondary amplifier of inflammation[16]. A recent study has demonstrated that high plasma level of S100A8/A9 at the early stage of sepsis is linked with a higher risk of death in septic shock patients[17]. Moreover, S100A8/A9 is an endogenous activator of toll-like receptor 4 (TLR4), regulating the inflammatory cascade during sepsis[16]. Platelet TLR4 detects its ligands in blood and induces platelets binding to adherent PMNs and formation of NETs[18]. However, the interaction between S100A8/A9 and platelets in the development of inflammation during sepsis remains unclear.

In the present study, we provide evidence for GSDMD-dependent platelet pyroptosis in severe sepsis using platelet-specific *Gsdmd* knockout (KO) mice. In severe sepsis, elevated S100A8/A9 induces GSDMD-dependent pyroptosis via a

TLR4/NLRP3 axis. Pyroptotic platelet-derived ox-mtDNA potentially promotes NET formation, which in turn contributes to platelet pyroptosis via release of S100A8/A9, forming a positive feedback loop that exacerbates inflammation in severe sepsis.

Results

Cohort characteristics and proteomic analysis of platelets from septic patients

On retrospective examination of the electronic medical records of sepsis (n = 37), severe sepsis (n = 22), septic shock (n = 34) and healthy subjects (HS) (n = 75), we found that children with severe sepsis/septic shock had moderate/severe complications (peripheral vascular, cerebrovascular, lung, liver, kidney, and heart) and high mortality rate (14% and 50%) on admission (Fig.1a), as reflected by higher score in acute physiology and chronic health evaluation (APACHE IV) scores (Table 1). On the contrary, patients with moderate sepsis had few complications and low death rates after appropriate treatment (Fig.1a). Plasma levels of proinflammatory cytokines (IL-1β, TNFα and IL-6) and procalcitonin (PCT) and C-reactivated protein (CRP) in septic patients, especially in severe sepsis/septic shock patients, were significantly increased compared to that of the HS group (Fig.1b and Table 1). Additionally, severe sepsis/septic shock patients had evidence of thrombocytopathy (high mean platelet volume (MPV), high platelet distribution width (PDW) and high platelet large cell ratio (P-LCR)), and coagulopathy (high activated partial thromboplastin time (APTT), prolonged prothrombin time (PT) and low fibrinogen (FIB)) (Fig.1c and Table 1).

106 The platelet counts in severe sepsis/septic shock patients were gradually
107 increased after admission, but remained lower compared to those in HS or mild sepsis
108 (Fig.1d). Based on such consistent features of severe sepsis/septic shock, and their
109 difference with moderate sepsis, we focused on severe sepsis (with or without septic
110 shock), who are collectively referred to as severe sepsis, in the following context
111 unless otherwise indicated. Collectively, these results support that the assessment of
112 platelet counts and morphology closely correlate with inflammation and pathology
113 severity in septic patients. The key questions arise as to whether abnormal platelets
114 could potentially offer an additional biomarker to assess severity of septic patients,
115 and the role of platelets in exacerbating severe sepsis.

116 To identify platelet changes associated with severe sepsis, purified platelet
117 samples from 3 severe sepsis and 3 HS were subjected to high-throughput proteomics
118 analysis using data-independent acquisition mass spectrometry (DIA-MS) (Fig.1e). A
119 total of 3189 proteins were identified across all the samples. Among all the 656
120 differentially expressed proteins (DEPs), 595 proteins were significantly up-regulated,
121 and 61 proteins were down-regulated in the septic group compared to that of HS
122 (Fig.1e). Pathway analysis of DEPs in platelets showed apoptosis (including
123 pyroptosis (pyroptosis related proteins also have been classified into apoptosis)) and
124 necroptosis pathways were significantly up-regulated in patients compared to HS
125 (Fig.1f). Representative proteins related to different cell deaths signal pathways were
126 displayed as a heat map. Proteins involved in the process of apoptosis (i.e., BAK, P =
127 0.002 etc.) and autophagy (i.e., LAMP2, P = 0.034 etc.) were increased (Extended

Data Fig.1a). The key pyroptosis related proteins including GSDMD (P = 0.007) was also increased in severe septic platelets (Fig.1g). Due to the heterogeneity of platelets in septic patients, fluorescence-activated cell sorter (FACS) analysis was performed to delineate the type of cell death pathway that was primarily present in the septic platelets. As shown in Fig.1h, 30.5% of platelets were apoptotic (caspase 3/7 positive platelets), 2.2% of platelets were autophagic (LC3B positive platelets), and 51.2% of platelets were pyroptotic (caspase 1 positive platelets). Platelet pyroptosis also ensued in mild sepsis, but mainly in severe sepsis (Extended Data Fig.1b). These data demonstrate pyroptosis to be the predominant form of cell death in platelets from severe sepsis.

GSDMD-dependent pyroptosis ensues in platelets from severe sepsis

Transmission electron microscopy (TEM) was used to determine the ultrastructure of platelets form severe sepsis patients and HS. Firstly, platelets were treated with different cell death agonists *in vitro* to identify the features of different cell death by TEM (Extended Data Fig.4a). In platelets from severe sepsis, in addition to some features of apoptosis (Extended Data Fig.4b), cell swelling, loss of cellular architecture, plasma membrane rupture and release of cytosolic contents, all characteristics of end stage pyroptosis[6] were found (Fig.2a). Immunofluorescence showed that NLRP3 inflammasome assembled with ASC in platelets from severe sepsis (Fig.2b and Extended Data Fig.3a). Additionally, caspase 1 activation was significantly increased in platelets from severe sepsis compared to that of HS platelets

(Fig.2c, e). Consistent with the results from DIA-MS, activated GSDMD (cleaved GSDMD-N) was significantly increased in platelets from severe sepsis compared to that of HS platelets (Fig.2d). Compared to that of HS, the level of platelet-derived IL-1β was significantly increased in platelets from severe sepsis (Fig.2f). These results suggest that platelet pyroptosis is activated in severe sepsis.

To further investigate the requirement of GSDMD for platelet pyroptosis, the platelet-specific *Gsdmd* KO (*Gsdmd*$^{fl/fl}$ PF4-Cre) mice were produced by crossing *Gsdmd*$^{fl/fl}$ mice with PF4-Cre mice (Extended Data Fig.4a, b). The parameters and classic functions (platelet activation and thrombosis/haemostasis) of platelets were not significantly different between platelet-specific *Gsdmd* KO mice and *Gsdmd*$^{fl/fl}$ mice (Supplementary Table 1 and Extended Data Fig.4c, d). After lipopolysaccharide (LPS) and Nigericin treatment (used as classical pyroptosis stimuli), the morphologic features of rapid swelling and membrane rupture were observed in platelets from the littermate controls, but was absent in the *Gsdmd* KO platelets (Fig.2g and Supplementary Video 1-2). Moreover, to assess the role of GSDMD for platelets pyroptosis *in vivo*, *Gsdmd*$^{fl/fl}$ PF4-Cre mice and *Gsdmd*$^{fl/fl}$ mice were subjected to the cecal ligation and puncture (CLP)-induced sepsis murine model. Swollen ruptured platelets with release of contents were observed via TEM in the *Gsdmd*$^{fl/fl}$ mice, but these changes were not seen in the *Gsdmd*$^{fl/fl}$ PF4-Cre mice (Fig.2h). These data suggest that GSDMD is required to trigger pyroptosis in septic platelets.

S100A8/A9 induces platelet pyroptosis through the TLR4 pathway

Consistent with previous studies[19], S100A8/A9 was significantly increased in severe sepsis patients (Extended Data Fig.5a). Similarly, S100A8/A9 was also significantly elevated in the CLP or LPS-induced sepsis mice (Extended Data Fig.5b, c). The percentage of pyroptotic platelets (activated caspase 1 positive platelets) positively correlated with the plasma levels of S100A8/A9 in severe sepsis patients (Fig.3a). Our *in vitro* result showed that NLRP3 inflammasome was assembled with ASC in platelets treated with recombinant human S100A8/A9 (rhS100A8/A9) compared to vehicle control (Fig.3b and Extended Data Fig.3b). Furthermore, activated caspase 1 (Fig.3c) and GSDMD (Fig.3d) were significantly increased in platelets treated with rhS100A8/A9 compared to vehicle control. *In vivo,* recombinant mouse S100A8/A9 (rmS100A8/A9) could induce platelet pyroptosis (activated caspase 1 positive platelets) like CLP (Extended Data Fig.5d).

Having observed that S100A8/A9 induced platelet pyroptosis, we sought to identify candidate platelet receptors of S100A8/A9. S100A8/A9 can regulate cell function by binding to cell surface receptors such as TLR4[16], advanced glycation end products (RAGE)[20] and CD36[21]. To determine which receptor participates in S100A8/A9-induced platelet pyroptosis, we evaluated platelet pyroptosis in the presence of neutralizing antibodies for CD36, RAGE or TLR4. Platelet pyroptosis was significantly suppressed by anti-TLR4 antibody compared to that observed with other neutralizing antibodies and isotype control (Extended Data Fig.6a). In addition, platelet activation was significantly inhibited by anti-CD36 antibody compared to that observed with other neutralizing antibodies and isotype control (Extended Data

Fig.6b), which is consistent with previous report[21]. Paquinimod (also known as ABR-215757) can prevent the binding of S100A9 to TLR4[22]. Blockade of S100A9 by Paquinimod significantly attenuated NLRP3 inflammasome formation (Fig.3b and Extended Data Fig.3b), the activation of caspase 1 (Fig.3c) and GSDMD (Fig.3d) in platelets.

To further determine whether TLR4 is involved in S100A8/A9-induced platelet pyroptosis, platelets (wild type (WT) or global *Tlr4* deficient (*Tlr4*$^{-/-}$), no significant differences in the parameters of platelets) (Supplementary Table 2) were treated with rmS100A8/A9. Compared to the vehicle group, the activation of caspase 1 was significantly attenuated in *Tlr4*$^{-/-}$ platelets treated with rmS100A8/A9 *in vitro* (Extended Data Fig.7a). Furthermore, *Tlr4*$^{-/-}$ platelets were transfused into mice to determine TLR4 function *in vivo*. To monitor transfused platelet dynamics, purified platelets from *Tlr4*$^{-/-}$ or WT mice were transfused intravenously into a mT/mG: PF4-Cre mouse[23], where PF4-Cre drives membrane GFP expression. After LPS treatment, a greater percentage of transfused *Tlr4*$^{-/-}$ platelets (GFP negative and CD41 positive cells) over total platelet counts (CD41 positive cells) were retained and detected in mice compared to that of mice transfused with WT platelets (Extended Data Fig.7b-d). NLRP3 inflammasome formation and activation of caspase 1 were significantly attenuated following *Tlr4*$^{-/-}$ platelet transfusion compared to transfusion with WT platelets (Fig.3e, f and Extended Data Fig.7e, f). Taken together, our results suggest that TLR4 is required for S100A8/A9-induced platelet pyroptosis.

213 Since mitochondrial ROS are activators of NLRP3 inflammasome[24], we then
214 assessed the mitochondrial function of septic platelets. Platelets isolated from severe
215 sepsis patients exhibited mitochondria dysfunction, as indicated by dissipation of $\Delta\psi_m$
216 (Extended Data Fig.8a) and increased mitochondrial ROS production (Fig.3g).
217 Blockade of mitochondrial ROS production with the mitochondrial specific
218 antioxidant MitoTempo significantly attenuated the induction of caspase 1 activity in
219 septic platelets (Fig.3h). Dissipation of $\Delta\psi_m$ and increased mitochondrial ROS
220 production were observed in platelets treated with rmS100A8/A9 *in vitro* (Fig.3i and
221 Extended Data Fig.8b, c) and *in vivo* (Extended Data Fig.8d, e), however, these
222 changes were not found in the *Tlr4*$^{-/-}$ platelets (Extended Data Fig.8). Our results
223 suggest that mitochondrial ROS are required for the activation of caspase 1 and
224 NLRP3 inflammasome.

225 **Pyroptotic platelets promote NET formation potentially through ox-mtDNA**
226 **release**

227 NET formation (as assessed by myeloperoxidase (MPO)-DNA complexes and
228 double-stranded DNA (dsDNA)) was significantly increased in the plasma of severe
229 sepsis patients (Fig.4a). NET formation positively correlated with the percentage of
230 pyroptotic platelets (activated caspase 1 positive platelets) in severe sepsis patients
231 (Fig.4b). When incubated with purified PMNs, either phorbol myristate acetate (PMA,
232 used as classical NET stimuli) or S100A8/A9-induced pyroptotic platelets, induced
233 NET formation (DNA and MPO double positive cells) with concomitant increased

MPO-DNA complexes and dsDNA, compared to PBS-treated and resting platelet-treated groups (Fig.4c, d), but not rhS100A8/A9 alone (Extended Data Fig.9a). In case of equivalent cells, the pyroptotic platelets could induce more NETs fromation than that of activated platelets (Extended Data Fig.9b-d). Since S100A8/A9-induced platelet pyroptosis via TLR4 (Fig.3), murine PMNs were incubated with rmS100A8/A9-treated murine platelets (WT or *Tlr4*$^{-/-}$) to assess for NET formation. RmS100A8/A9-induced *Tlr4*$^{-/-}$ platelets had significantly reduced NET formation compared to WT platelets (Fig.4e, f). These results suggest that S100A8/A9-induced platelet pyroptosis contributes to NET formation.

Since ox-mtDNA participates in NET formation[12], we wondered whether platelet-derived ox-mtDNA could induce NET formation. Firstly, we found supernatants of rhS100A8/A9-induced platelets could induce NETs formation (Extended Data Fig.9a), indicating pyroptotic platelets may induce NETs formation without direct interaction with PMNs. Moreover, we found that levels of DNA 8-Oxo-2'-deoxyguanosine (8-OHdG) were significantly increased in the supernatant of S100A8/A9-treated platelets (Fig.4g), indicative of platelet-derived ox-mtDNA release. The increased DNA 8-OHdG was significantly attenuated in rmS100A8/A9-induced *Gsdmd* KO platelets compared to that of control (Fig.4g). Furthermore, ox-mtDNA level was significantly increased in the plasma of severe sepsis patients (Fig.4h) and CLP-induced mice (Fig.4i). These results suggest that S100A8/A9-induced platelet pyroptosis releases ox-mtDNA, which may induce NET formation in severe sepsis.

NET formation in turn induces platelet pyroptosis via the release of S100A8/A9

Consistent with previous studies[14], S100A8/A9 was significantly increased in the PMA or rhS100A8/A9-induced pyroptotic platelets induced NETs (Fig.5a). To determine whether NET-derived S100A8/A9 induce platelet pyroptosis, murine platelets were incubated with PMA-treated murine PMNs (WT or global *S100a9* deficient (*S100a9*$^{-/-}$)). Immunofluorescence demonstrated pyroptotic platelets (caspase 1 positive cells) in the net structure of NETs (Fig.5b and Extended Data Fig.9e). Platelet pyroptosis, as indicated by mitochondrial ROS, NLRP3 inflammasome and activated caspase 1, was significantly reduced when incubated with *S100a9*$^{-/-}$ PMNs, compared to WT PMNs (Fig.5c-f). These results suggest that NET-derived S100A8/A9 contributes to platelet pyroptosis.

Gsdmd deficiency in platelets ameliorates excessive NET-mediated inflammation in sepsis mice

To address the role of GSDMD-dependent platelet pyroptosis in NET formation in severe sepsis, platelets isolated from *Gsdmd*$^{fl/fl}$ PF4-Cre mice and *Gsdmd*$^{fl/fl}$ mice were treated with rmS100A8/A9 to induce pyroptosis, followed by incubation with murine PMNs. Incubation with rmS100A8/A9-treated *Gsdmd*$^{fl/fl}$ platelets induced NET formation, as indicated by DNA and MPO double positive cells, but this was not observed in the *Gsdmd*$^{fl/fl}$ KO platelets (Fig.6a). Moreover, NET formation was also significantly decreased in rmS100A8/A9-induced *Gsdmd* KO platelets (Fig.6b, c). *In vivo*, NET formation in *Gsdmd*$^{fl/fl}$ PF4-Cre mice was significantly attenuated

277 compared to that of *Gsdmd*$^{fl/fl}$ mice by CLP (Fig.6d, e). Consistent with the patient
278 results (Fig.1b), the proinflammatory cytokines were significantly increased in
279 *Gsdmd*$^{fl/fl}$ mice, while were significantly reduced in *Gsdmd*$^{fl/fl}$ PF4-Cre mice by CLP
280 (Fig.6f-h). Moreover, the mortality of *Gsdmd*$^{fl/fl}$ PF4-Cre mice was significantly
281 reduced compared to that of *Gsdmd*$^{fl/fl}$ mice by CLP (Fig.6i). Our results suggest that
282 GSDMD-dependent platelet pyroptosis contributes to NET formation, the enhanced
283 inflammation and mortality associated with severe sepsis.

284 In addition to inflammation, the development of thrombocytopenia during a
285 septic episode is recognized as a significant event associated with multiple organ
286 failure and increased mortality[3]. Upon admission, 60% of septic patients developed
287 severe sepsis, of which platelet counts remained low over 28 days (Fig.1d), consistent
288 with previous studies[25]. The *Gsdmd*$^{fl/fl}$ PF4-Cre mice demonstrated a small but
289 non-significant increase in platelet counts (Extended Data Fig.10), suggesting that
290 GSDMD-dependent pyroptosis is not a major contributor to the thrombocytopenia.
291 Our data supports a key role for GSDMD-dependent platelet pyroptosis in NET
292 formation and inflammation in severe sepsis, but not thrombocytopenia.

293 **Paquinimod ameliorates NET-mediated inflammation and improves survival**
294 **rate by suppressing platelet pyroptosis**

295 To establish whether a platelet S100A8/A9-TLR4 axis may provide therapeutic
296 benefit for inflammation progression in severe sepsis, pharmacologic inhibition of
297 S100A9 (Paquinimod) was introduced to the CLP-induced sepsis mice. Consistent

with the patients result (Extended Data Fig.5a, Fig.3g and Fig.2e), we found that the plasma S100A8/A9, mitochondrial ROS and caspase 1 activity were significantly increased in sepsis mice, however, these were significant reduction in sepsis mice with Paquinimod treatment (Fig.7a-c). Administration of Paquinimod also significantly reduced NETs formation in the plasma of sepsis mice (Fig.7d, e), as well as significantly suppressed the plasma level of proinflammatory cytokines (Fig.7f-h). Compared to PBS-treated mice, administration of Paquinimod significantly increased survival rate in sepsis mice (Fig.7i). Taken together, these results indicate that pharmacological inhibition of the S100A8/A9 with Paquinimod suppresses platelet pyroptosis, thereby ameliorating NET formation and inflammation, consequently leading to increased survival in sepsis.

Discussion

Sepsis is a time critical emergency, which can rapidly spiral to severe sepsis[26]. Thus, early recognition is required. The underlying mechanisms for such rapid progression are poorly understood, leading to lack of effective therapies. With the use of three different genetic modified murine models (*Gsdmd*$^{-/-}$, *Tlr4*$^{-/-}$ and *S100a9*$^{-/-}$), we now demonstrate that sepsis-derived S100A8/A9 induces GSDMD-dependent platelet pyroptosis via the TLR4/ROS/NLRP3/caspase 1 pathway, leading to the release of ox-mtDNA to mediate NET formation. Furthermore, we find that NET in turn release S100A8/A9 and accelerate platelet pyroptosis, forming a positive feedback loop, thereby amplifying the production of proinflammatory cytokines. *Gsdmd* deficiency

in platelets or pharmacological inhibition of S100A9 using Paquinimod can break this detrimental feedback loop, thus ameliorating excessive NET-mediated inflammation in severe sepsis (Fig 8).

The first report of GSDMD-dependent platelet pyroptosis in sepsis

Pyroptosis, as a form of inflammatory cell death, has been well documented in different cell types of various diseases[6,27]. However, it remains uncertain whether pyroptosis ensues in platelets during sepsis. In the CLP-induced sepsis, NLRP3 inflammasome was activated in platelets and the levels of IL-1β/IL-18 significantly increased, which were associated with inflammation and multiple organ injury[7]. Moreover, NLRP3 inflammasome inhibition normalized these cytokine levels and prevented multiple organ injury[28]. A recent study indicated the activated NLRP3 inflammasome may be involved in primary immune thrombocytopenia via the ROS-NLRP3-caspase-1 pathway[8]. On the contrary, another study suggested that human and mouse platelets did not express the components (NLRP3, ASC, caspase-1, or IL-1β) of the canonical pathways of inflammasome activation[29], and the discrepancy may be due to the severity of different diseases. Thus, it is important to verify whether platelets have NLPR3 inflammasome and if so whether platelet pyroptosis serves a pathophysiological role. Using DIA-MS, immunofluorescence and western blotting, we confirmed the expression of NLRP3, ASC and GSDMD in platelets. Furthermore, with the use of platelet-specific *Gsdmd* KO mice, we provided direct evidence that GSDMD is a key component for platelet

pyroptosis in sepsis (Fig.2).

Our study demonstrates the importance of the S100A8/A9-TLR4 signaling pathway in platelet pyroptosis during sepsis. Through blocking TLR4 signaling with TLR4 antibody, *Tlr4*$^{-/-}$ platelet transfusion, or Paquinimod, we suppressed platelet pyroptosis and improved survival rate in CLP-induced sepsis mice. A recent study also showed that S100A8/A9 mediated activation of aberrant PMNs and immune disorder through TLR4 in the pathogenesis of COVID-19[30]. Although many studies have realized the important role of S100A8/A9 in sepsis[31,32], the underlying mechanism was not clear. Here, we found the new role of S100A8/A9 in platelet pyroptosis during severe sepsis via TLR4 signaling pathway.

The clinical outcomes of pediatric severe sepsis including excessive inflammation and thrombocytopenia are the major causes of mortality in severe sepsis[3]. Our result that substantial platelet pyroptosis leads to increased IL-1β release (Fig.2f), is supported by recent studies that platelet-derived IL-1β mediates endothelium permeability in dengue[33], which amplifies the proinflammatory cytokine production in the plasma of severe patients (Fig.1b). On the other hand, in our cohort the platelet counts in severe sepsis patients remained low after admission (Fig.1d). Thrombocytopenia in severe sepsis is caused by altered platelet production, hemophagocytosis, antibodies, disseminated intravascular coagulation (DIC), or platelet scavenging in the circulation due to platelet-leukocyte or platelet-pathogen interactions, vessel injury, or desialylation[34]. A recent report suggested that elevated

angiotensin II induced platelet apoptosis, leading to sepsis-associated thrombocytopenia[35]. In our study, GSDMD-dependent pyroptosis slightly reduces the platelet counts, but it is not a major contributor to thrombocytopenia in sepsis.

A positive feedback loop between platelets and NETs to amplify inflammation

The crosstalk between PMNs and platelets depends on cell-to-cell contact and secreted substances, which activate each other[36]. Activated platelets have been shown to be potent activators of NETs by platelet-derived high mobility group box 1 (HMGB1), von Willebrand factor (vWF), platelet factor 4 (PF4) and exosomes[36,37]. NETs play a key role in killing pathogens, while excessive formation of NETs might exert tissue damage[36,38]. It has also been reported that NETs release S100A8/A9[14]. Here we propose that activated platelets promote NETs formation to kill pathogens at the early stage of sepsis. However, with the occurrence of platelet pyroptosis at the later stage of sepsis, excessive formation of NETs exacerbates the inflammatory response (e.g. release of S100A8/A9), which further induces platelet pyroptosis, forming a positive feedback loop between platelets and NETs (Fig 4-6). Our study provide a novel insight into the mechanism of S100A8/A9-induced platelet pyroptosis inducing NET formation in sepsis.

Therapeutic implications in severe sepsis

Rapidly dysregulated immune systems and prolonged excessive inflammation induce multi-organ failure and increased mortality[39]. Standard treatments require the

combination of anti-microbial therapy, supportive care including fluid therapy, and/or vasoactive pressor medications[1]. Despite such therapies, 60% of our recruited septic patients developed severe complications, suggesting that alternative therapies are urgently needed for such severe sepsis. Potent disease-inhibitory effects of Paquinimod have been suggested for experimental models of autoimmune and inflammation disease[40] and systemic lupus erythematosus[41]. Moreover, a recent study has suggested that inhibition of S100A9 with Paquinimod may reduce mortality and improved learning and memory performance in mice with sepsis[42]. We now provide an unusual mechanism involving a platelet pyroptosis positive feedback loop that contributes to the development of severe sepsis. In CLP-induced sepsis mice, our results showed that administration of Paquinimod effectively suppressed platelet pyroptosis and NET formation, with concomitant reduced inflammation, resulting in improved survival rate (Fig.7). Therefore, targeting S100A8/A9-TLR4 pathway may provide a novel adjunct therapy for inflammation progression in septic patients.

In summary, S100A8/A9 induces GSDMD-dependent platelet pyroptosis via TLR4/NLRP3 pathway in severe sepsis, which exacerbates NET formation via the release of ox-mtDNA. NETs in turn release S100A8/A9, thereby inducing platelet pyroptosis in severe sepsis (Fig 8). This positive feedback mechanism contributes to the amplification of inflammation following infection. Thus, assessment of platelet pyroptosis may serve as a diagnostic and prognostic tool for the progression of severe sepsis. Particularly in patients with severe sepsis and with substantial platelets

402 pyroptosis, targeting S100A8/A9 or platelet-specific GSDMD may provide a much
403 needed adjunct therapy.

Methods

Patient recruitment and isolation of human platelets

We recruited 93 pediatric sepsis patients (0-18 ages) and 75 age-matched HS, who were from Guangzhou Women and Children's Medical Center, Guangzhou Medical University, China from November 2019 to August 2021 (**Table 1**). According to international guidelines[43], pediatric sepsis is defined by its systemic inflammatory response syndrome plus suspected or proven infection. Positive cultures of bacteria or fungi in blood samples from patients are the gold standard. Clinical signs include at least two of the following criteria: ① temperature < 36℃ or > 38℃, ② white blood cell (WBC) counts ≥ 34×10^9/L or ＜5×10^9/L, ③ thrombocytopenia (platelet counts < 100,000 μL^{-1}), ④ respiratory rate > 20 breaths/minute, PaO_2 < 4.3 kPa (32 mmHg). According to clinical spectrum of severity, it encompasses sepsis (systemic inflammatory response syndrome in the presence of infection), severe sepsis (sepsis in the presence of cardiovascular dysfunction, acute respiratory distress syndrome, or dysfunction of ≥ 2 organ systems) and septic shock (sepsis with cardiovascular dysfunction persisting after at least 40 ml/kg of fluid resuscitation in one hour). Informed consent for underage subjects was obtained from their parents or legal guardians. The ages of patients with sepsis were 0 to 18 years old, which are divided into 0~1 year, 1~5 years, 5-12 years and 12-18 years. The study was approved by the Institutional Review Board of Guangzhou Women and Children's Medical Center and informed consent was obtained from each subject (Human Investigation Committee

No. 2019-44102-1). Informed consent was obtained from each subject, and the human studies conformed to the principles set out in the World Medical Association (WMA) Declaration of Helsinki.

All the patients with sepsis were treated with antibiotics including cephalosporin, vancomycin and broad-spectrum penicillin after admission. Venous blood samples were drawn from septic patients when they were enrolled first day. Venous blood samples (3 ml) were drawn from HS and severe sepsis patients with blood collection tubes containing 3.8% trisodium citrate (w/v), and prepared as previously described[44]. Briefly, platelet-rich plasma (PRP) was centrifuged at 250 g at 25°C for 15 minutes. PRP were then treated with 100 nM prostaglandin E1 (PGE1, Sigma, 745-65-3) and centrifuged at 1000 g for 5 minutes. After discarding the supernatant, the platelet pellet was washed and resuspended with 3 ml Hank's Balanced Salt Solution (HBSS, Gibco, 14025092). Purity of platelet preparation was determined by FACS (BD, FACS Canto^{TM}) analysis using platelet markers (>90% FITC anti-human CD41a, BD, 555466). Platelets at the concentration of 10^8 platelets/ml were used in experiments.

Animal and Treatment

The *Gsdmd*$^{flox/flox}$ murine model used in this study was designed and developed by Shanghai Model Organisms Center, Inc (Shanghai, China). Briefly, the targeting construct was designed to flank exon 3 with loxP sites and a pGK-Neomycine-polyA cassette. The targeting vector was electroporated into C57BL/6J embryonic stem cells (ES), which were performed double drug selection with G418 and ganciclovir for

screening the homologous recombination clones. The ES clones with correct homologous recombination were identified by PCR and confirmed by sequencing. Positive ES cell clones were expanded and microinjected into C57BL/6J blastocysts to generate the chimeric offsprings. The platelet-specific *Gsdmd* KO mice (*Gsdmd*$^{flox/flox}$ PF4-Cre) were generated by crossing the *Gsdmd* flox and PF4-Cre. Mice were genotyped using primers P8 (5'-AGGGCGTCAGATCTCATTACAG-3') and P9 (5'- TTCCCATCGACGACATCAGAGACT-3').

The global *S100a9* deficient (*S100a9*$^{-/-}$) mice model used in this study was designed and developed by Shanghai Model Organisms Center, Inc (Shanghai, China). Briefly, Cas9 mRNA was *in vitro* transcribed with mMESSAGE mMACHINE T7 Ultra Kit (Ambion, TX, USA) according to the manufacturer's instructions. Two sgRNAs targeted to delete exons 2-3 were *in vitro* transcribed using the MEGAshortscript Kit (ThermoFisher, USA, B135410). One sgRNA targeted to intron 1 of gene *S100a9* was 5'- CAGTGGCCAGAGACTAGGTCAGG-3. The other sgRNA targeted to 3' downstream sequence of gene *S100a9* was 5'-GGTTCTCACATGAATGGGAATGG -3'. *In vitro*-transcribed Cas9 mRNA and sgRNAs were injected into zygotes of C57BL/6J mouse, which were transferred to pseudopregnant recipients. Obtained F0 mice were validated by PCR and sequencing using primer pairs: F (5'-TCAGATGCAAGGGGGAGAATG-3') and R (5'-GGGGGTCACTTGATCTCTTTGGTC-3'). The positive F0 mice were chosen and crossed with C57BL/6J mice to obtain F1 heterozygous *S100a9*$^{-/-}$ mice. The genotype of F1 mice was identified by PCR and confirmed by sequencing. Male and female F1

heterozygous mice were intercrossed to produce the homozygous *S100a9*$^{-/-}$ mice.

The global *Tlr4* deficient (*Tlr4*$^{-/-}$) mice, mT/mG: PF4-Cre mice and WT mice were obtained from the Jackson Laboratory and backcrossed to C57BL/6 mice (Bar Harbor, USA). Genotyping was performed via PCR using standard methods. To block S100A8/A9-TLR4 axis, five-week-old mice were gavaged with Paquinimod (synonyms: ABR-215757; 10 mg/kg/day, MedChemExpress, HY-100442) or PBS (HyClone, SH30258.01) every 24 hours over 5 days (n = 6/group). To build a murine septic model, five-week-old mice were induced by CLP with 19-gauge needle as described[45]. Briefly, the cecum was ligated at the designated position for the desired severity grade, and then ligation of the ileocecal valve was subjected to a single through-and-through puncture with 19-gauge needle. Sham-operated mice underwent the same surgical procedure except for ligation and perforation of the cecum. To build LPS-induced septic shock model, five-week-old mice were injected a single dose of 20 mg/kg LPS (Sigma, L4391) (n = 6/group). Mice were housed in pathogen-free conditions in Guangzhou Medical University animal facilities. Procedures were approved by the Institutional Animal Care and Use Committee of Guangzhou Medical University (No. SYXK2018-266). All mice experiments complied with the principle of animal protection, welfare, ethics and 3R (Replacement, Reduce and Refine).

DIA-MS

Purified platelets were obtained from severe sepsis patients and HS as described above. Library-based DIA analysis strategy was adopted in this study. Eluted peptides

were sprayed directly into the nanoESI source and then entered a Q-Exactive HF X mass spectrometer (Thermo Fisher Scientific San Jose, CA) for DDA and DIA data acquisition. Spectral library was generated from MaxQuant DDA search results using Spectronaut with default settings. With the established spectral library, the acquired DIA data were processed and analyzed by Spectronaut, with retention time prediction type set to dynamic iRT, decoy generation set to scambled, peptide and protein level Q-value cutoff set to 1% and Normalization Strategy set to Local Normalization. The precursor level of Spectronaut normal report was exported, and downstream data process including log-transformed intensities, median normalization across conditions, and protein summarization were performed using MSstats. Based on the preset comparison groups, the mixed linear model in MSstats was employed to assess DEPs. The criteria of fold change > 1.5 and P value < 0.05 were used to determine the statistically significant differences. Heatmap of all significant DEPs was performed using the Euclidean distance and Hierarchical Cluster.

TEM

To distinguish morphologic features of pyroptosis from apoptosis, platelets were examined by TEM. Platelets were fixed and stained according to previously described[46]. The ultrastructural sections were examined with the TEM FEI CM100 (Japan Electron Optics Laboratory), followed captured with an Advantage CCD camera using iTEM software (Olympus).

In vivo platelet depletion and transfusion assay

Blocking TLR4 signaling by transfusion of *Tlr4*$^{-/-}$ platelets into WT mice can be an effective method to verify the role of TLR4 in platelets during sepsis[47,48]. Platelets were depleted from C57BL/6J mice as previously described[48]. Briefly, five-week-old mice were injected intravenously at 5 μl/mouse with rabbit anti-mouse thrombocyte polyclonal antibody (Mybiosource, MBS524066) or normal saline (volume: 200 μl) before experiments. After 24 hours post ablation (reduction of platelets without affecting leukocytes), blood samples (approximately 0.8 ml) were directly obtained from the right cardiac ventricle into 3.8% trisodium citrate in mice. Obtained blood samples were diluted with equal volume of HBSS buffer (3 ml). PRP was centrifuged at 250 g at 25°C for 5 minutes. PRP was recentrifuged at 1000 g for 5 minutes containing 100 nM PGE1. After discarding the supernatant, the platelet pellet was washed and resuspended with 3 ml HBSS. According to the reference[49,50], a total of 1.2×10^7 purified platelets (volume: 200 μl, concentration: 6×10^{10} platelets/L) were transfused intravenously to recipient mice. *Tlr4*$^{-/-}$ platelets and WT platelets were transfused intravenously to recipient mice, followed by LPS induced sepsis for 6 hours (n = 6/group). Mouse anaesthesia were euthanized by chloral hydrate in PBS at a dose of 400~500 mg/kg after post-infection, and then experimented for retro-orbital blood drawls. Whole blood was collected by cardiac puncture. After finishing all experiments, mice were euthanized by CO_2 asphyxiation. For platelet counts, mice were bled from the retro-orbital plexus. Platelet count in whole blood was analyzed using a hematology analyzer[47] (Sysmex Corporation, XN-350).

In a murine model, exogenous platelets isolated from *Tlr4*$^{-/-}$ mice were

transfused into platelet-depleted mice achieved by rabbit anti-mouse thrombocyte polyclonal antibody to keep the physiologic platelet level. To monitor transfused platelet dynamics, purified platelets were prepared and a total of 1.2 x 10^7 purified platelets (volume: 200 μl, concentration: 6 x 10^{10} platelets/L) from *Tlr4*$^{-/-}$ or WT mice were transfused intravenously to a mT/mG: PF4-Cre murine model, in which PF4-Cre drives membrane GFP expression in megakaryocytes and platelets, while all other cells are labeled with mT[23]. For platelet counts, mice were bled from the retro-orbital plexus during LPS-induced sepsis. After platelets depletion, platelet counts in mice transfused with WT or *Tlr4*$^{-/-}$ platelets were detected at 0, 0.5, 2, 4 and 6 hours using a hematology analyzer. The platelets from mice were stained with PE-Cy7 anti-mouse CD41 (Thermo Fisher, 25-0411-82) and detected at 0, 0.5, 2, 4 and 6 hours using FACS.

Isolation of human and murine PMNs

PMNs were isolated from the peripheral blood of HS as previously described[51]. PMNs were obtained with Ficoll Hypaque gradient centrifugation (δ = 10771, Sigma), according to the manufacturer's instructions. The red blood cell (RBC) layer was then ablated by hypotonic lysis. Cell suspensions contained 95% PMNs, as determined by APC anti-human CD66b antibodies (BioLegend, 305118) staining and FACS. The cells were washed in PBS and resuspended with RPMI 1640 (contained with 2% FBS, Gibco, 10099141C). Murine PMNs were obtained with Ficoll Hypaque gradient centrifugation (δ = 1090, Sigma), according to the manufacturer's instructions. The RBC layer was then ablated by hypotonic lysis. Cell suspensions contained 90%

554 PMNs, as determined by PE anti-mouse Ly6G (BioLegend, 127607) staining and
555 FACS. The cells were washed in PBS and resuspended with RPMI 1640 (contained
556 with 2% FBS, Gibco, 10099141C). The PMNs were used for immunofluorescence
557 analysis assays.

558 **NET formation and imaging assay**

559 NET formation was evaluated as previously described[52]. To identify the association
560 between NET formation and platelet pyroptosis, purified human PMNs (2 x 10^5/ml)
561 were pre-stimulated with phorbol myristate acetate (PMA, 50 nM, Sigma, P1585) that
562 used as classical NET stimuli for subsequent assessments, resting platelets or
563 pyroptotic platelets (1 μg/ml rhS100A8/A9-induced, BioLegend, 753404) (0.04 x
564 10^5/ml) for 4 hours. To further confirm that pyroptotic platelets triggered NET
565 formation purified murine PMNs (2 x 10^5/ml) were co-cultured with resting WT
566 platelets or co-cultured with rmS100A8/A9-induced (1 μg/ml, BioLegend, 765506)
567 *Tlr4*$^{-/-}$ platelets (0.04 x 10^5/ml) for 4 hours.

568 **Measurement of NETs**

569 To quantify NETs in plasma of human/mice and medium supernatant, dsDNA was
570 measured in severe sepsis using Quant-iT PicoGreen dsDNA reagent (Invitrogen,
571 P7581) according to the manufacturer's protocol. MPO-DNA complexes in plasma of
572 human/mice and medium supernatant were detected by anti-MPO polyclonal (Biotin
573 Conjugated) primary antibody (Bioss，bs-4943R-Biotin) and Cell Death Detection
574 ELISA kit (Roche, 11774425001)[53]. Briefly, anti-MPO polyclonal primary antibody

was as a capture antibody and peroxidase-labeled anti-DNA primary antibody as a detection antibody to test MPO-DNA complexes. The data were presented as percent of control ± SD, arbitrarily set at 100%.

ELISA assay

The level of heterodimer S100A8/A9, IL-1β, TNFα and IL-6 in plasma of human (S100A8/A9, CUSABIO CSB-E12149; IL-1β, BOSTER EK0392; IL-6, CUSABIO CSB-E04638h; TNF-α, CSB-E04740h) or mice (after 6 hours or 5 days of CLP operation; S100A8/A9, CUSABIO CSB-EQ013485MO; TNF-α, CSB-E04741m; IL-6, CSB-E04639m; IL-1β, EK0394 Mouse) were detected using ELISA kits according to the manufacturer's instructions. Concentrations of DNA 8-Hydroxydeoxyguanosine (8-OHdG) in Plasma or medium supernatant were measured by General 8-OHdG ELISA Kit (Develop, DL-8-OHdG-Ge), according to the manufacturer's instructions.

Immunofluorescence

Platelets or PMNs were fixed and incubated with antibodies including goat polyclonal anti-NLRP3 (Abcam, 1:100, ab4207), rabbit polyclonal anti-ASC (Novusbio, 1:100, NBP1-78978), rabbit monoclonal anti-CD41 (Abcam, 1:200, ab134131), Alexa Fluor 488 Anti-mouse CD41 (BioLegend, 1:200, 133908), Hoechst (Thermo, 1:3000, H3570), mouse monoclonal anti-myeloperoxidase (Genetx, 1:200, gtx75318), rabbit monoclonal anti-myeloperoxidase (Abcam, 1:200, ab208670) and rabbit polyclonal anti-Histone H3 (citrulline R2 + R8 + R17, Abcam, ab5103) at 4°C overnight. Secondary antibodies include Alexa Fluor 647-conjugated anti-goat secondary

antibody (Abcam, 1:200, ab150135), Alexa Fluor 647-conjugated anti-rabbit IgG secondary antibody (Abcam, 1:200, ab150079), Alexa Fluor 594-conjugated anti-rabbit IgG secondary antibody (BioLegend, 1:200, 403006), Alexa Fluor 594-conjugated anti-mouse IgG secondary antibody (Abcam, 1:200, ab150116), Alexa Fluor 488-conjugated anti-goat IgG secondary antibody (BioLegend, 1:200, 405508), Alexa Fluor 488-conjugated anti-rabbit IgG secondary antibody (Abcam, 1:200, ab150077) and Alexa Fluor 488-conjugated anti-mouse IgG secondary antibody (Abcam, 1:200, ab150113). Then, the cells were captured with immunofluorescence confocal microscopy (x63 oil immersion lens, Leica SP8).

Flow cytometric analysis

The Caspases 1, Caspase 3/7, LC3B and GSDMD activity of platelets were determined using Pyroptosis/Caspase-1 Assay (Green) kit (Immuno Chemistry, 1:200, #9146), FAM-FLICA® Caspase-3/7 Assay Kit (Immuno Chemistry, 1:200, #94), FLICA® 660 Caspase-3/7 Assay Kit (Immuno Chemistry, 1:200, #9125), LC3B antibody Alexa Fluor® 405 (NOVUSBIO, 1:200, NB100-2220AF405) and Alexa Fluor 594-conjugated anti-rabbit IgG secondary antibody (BioLegend, 1:200, 403006) according to the manufacturer's instructions. Platelet suspensions (10^8 platelets/ml) were incubated with antibodies at 37°C for 1 hour and analyzed by FACS. Each sample was analyzed using FACS. Data was collected from 20,000 platelets on a BD FACS CantoTM and analyzed using the FlowJo-V10 software.

Measurement of mitochondrial function

The mitochondrial membrane potential (ΔΨm) was detected by FACS. ΔΨm was measured by staining with 100 nM tetramethylrhodamine methyl ester (TMRM) (Invitrogen, T668) at 37°C for 30 minutes at room temperature. ROS levels were measured by a mitochondrial ROS detection kit according to the manufacturer's instructions. Mitochondrial superoxide production was labeled with 5 μM MitoSOXTM Red (Invitrogen, M36008) for 30 minutes at 37°C. Blockade of mitochondrial ROS production, the platelets were pre-incubated with 5 mM MitoTempo (Sigma, SML0737) for 1 hour. Changes in fluorescence intensity were determined by FACS as above.

Western blotting

Cells were collected and lysed using protein lysis buffer containing a protease inhibitor cocktail (Millipore, USA). Total proteins were separated by 12% SDS-PAGE and then transferred to PVDF membranes (Millipore, Billerica, MA, USA). Non-specific binding was blocked with 5% non-fat milk dissolved in Tris-buffered PBS with Tween 20 (TBST; 150 mM NaCl, 20 mM Tris-HCl, 0.1% Tween 20, pH 7.5) at room temperature for 2 hours. The membranes were incubated with the following primary antibodies overnight at 4 °C: polyclonal rabbit anti-GSDMD (Cell Signaling Technology, 1:1000, #96458S; or mouse, Abcam, 1:1000, ab209845), anti-NLRP3 (Cell Signaling Technology, 1:1000, #15101S), anti-TMS1/ASC (Abcam, 1:1000, ab151700), anti-pro Caspase 1 + p10 + p12 (Abcam, 1:1000, ab179515), α-Actinin (Abcam, 1:3000, ab68194) and β-Actin (Abcam, 1:3000, ab6276). The membranes were incubated with an appropriate secondary antibody (1:2000) dissolved in 5%

non-fat milk. The signals were visualized using ECL (Millipore, Billerica, MA, USA). Relative intensities were quantified using Image Lab (Bio-Rad).

Statistical Analysis

For the experimental data, statistical analyses and graphics production was performed using Graph Pad Prism v.8.0 (GraphPad, La Jolla, CA, USA). Continuous variables were expressed as mean and SD or median with interquartile range. Shapiro–Wilk test was used to determine normality of data. For normally distributed data, comparisons between two groups were analyzed using unpaired nonparametric Student's t-test. Comparisons between more than two groups were analyzed using one-way ANOVA analysis with the Tukey's multiple comparisons. For data that were not distributed normally, values were expressed as medians and interquartile ranges. Comparisons between two groups were analyzed using Mann-Whitney test and compared between more than two groups were performed with Kruskall-Wallis with Dunn multiple test. Comparisons between more than two groups were analyzed using two-way ANOVA analysis. Categorical variables were presented as frequency rates and percentages and analyzed using Chi-square test or Fisher's exact test as appropriate. Pearson's correlation test was used to analyze linear relationship between two variables. Log-rank (Mantel-Cox) test for survival curves. P value of 0.05 or less was considered statistically significant.

Author Contributions

MS, JH and WHT conceptualized the project; MS designed and performed most of

experiments; CC, SL, ZZ, LX, XF, QL, YW, YL, YB, YZ, JQ, MG, MQ and LS performed, or helped in the interpretation and design of some key experiments; MS, CC and WHT wrote the original manuscript draft; PW, ML, XL, WL, FC and DZ recruited and provided patient care and clinical assessments; RL, JH and WHT reviewed and edited the manuscript; WHT, MS, CC and ZZ acquired funding; WHT and JH provided resources and supervised the study. All authors provided critical comments on the manuscript.

Acknowledgments

This work was supported by the National Natural Science Foundation of China (Grant No. 82100141, 82101655, 82022003, 81970437 and 81903605), Natural Science Foundation of Guangdong Province (Grant No. 2021A1515011304), Guangzhou Science and Technology Project (Grant No. 202102020164 and 202102010151), Guangzhou Science and Post-doctoral Research Project (Grant No. 2180157 and 011302031), China Postdoctoral Science Foundation (2021M700934), Guangzhou Women and Children's Medical Center/Guangzhou Institute of Pediatrics (Grant No. 3001076 and 3001149).

Data availability

The datasets generated and/or analyzed during the current study are available in the source data file.

679 **References**

680 1. Weiss, S.L.*, et al.* Surviving sepsis campaign international guidelines for the
681 management of septic shock and sepsis-associated organ dysfunction in
682 children. *Intensive Care Med* **46**, 10-67 (2020).

683 2. Rudd, K.E.*, et al.* Global, regional, and national sepsis incidence and mortality,
684 1990-2017: analysis for the Global Burden of Disease Study. *Lancet* **395**,
685 200-211 (2020).

686 3. Kaukonen, K.M., Bailey, M., Pilcher, D., Cooper, D.J. & Bellomo, R.
687 Systemic inflammatory response syndrome criteria in defining severe sepsis. *N*
688 *Engl J Med* **372**, 1629-1638 (2015).

689 4. Vardon-Bounes, F.*, et al.* Platelets Are Critical Key Players in Sepsis. *Int J*
690 *Mol Sci* **20**(2019).

691 5. Shi, J.*, et al.* Cleavage of GSDMD by inflammatory caspases determines
692 pyroptotic cell death. *Nature* **526**, 660-665 (2015).

693 6. Jorgensen, I. & Miao, E.A. Pyroptotic cell death defends against intracellular
694 pathogens. *Immunol Rev* **265**, 130-142 (2015).

695 7. Cornelius, D.C.*, et al.* NLRP3 inflammasome activation in platelets in
696 response to sepsis. *Physiol Rep* **7**, e14073 (2019).

697 8. Wang, S.*, et al.* Reduced intracellular antioxidant capacity in platelets
698 contributes to primary immune thrombocytopenia via ROS-NLRP3-caspase-1
699 pathway. *Thromb Res* **199**, 1-9 (2021).

700 9. Neuwirt, E.*, et al.* NLRP3 as a sensor of metabolism gone awry. *Curr Opin*
701 *Biotechnol* **68**, 300-309 (2021).

702 10. Oka, T.*, et al.* Mitochondrial DNA that escapes from autophagy causes
703 inflammation and heart failure. *Nature* **485**, 251-255 (2012).

704 11. Shimada, K.*, et al.* Oxidized mitochondrial DNA activates the NLRP3
705 inflammasome during apoptosis. *Immunity* **36**, 401-414 (2012).

706 12. Lood, C.*, et al.* Neutrophil extracellular traps enriched in oxidized

707 mitochondrial DNA are interferogenic and contribute to lupus-like disease.
708 *Nat Med* **22**, 146-153 (2016).
709 13. Kaplan, M.J. & Radic, M. Neutrophil extracellular traps: double-edged swords
710 of innate immunity. *J Immunol* **189**, 2689-2695 (2012).
711 14. Sreejit, G.*, et al.* Neutrophil-Derived S100A8/A9 Amplify Granulopoiesis
712 After Myocardial Infarction. *Circulation* **141**, 1080-1094 (2020).
713 15. Nagareddy, P.R.*, et al.* NETosis Is Required for S100A8/A9-Induced
714 Granulopoiesis After Myocardial Infarction. *Arterioscler Thromb Vasc Biol* **40**,
715 2805-2807 (2020).
716 16. Vogl, T.*, et al.* Mrp8 and Mrp14 are endogenous activators of Toll-like
717 receptor 4, promoting lethal, endotoxin-induced shock. *Nat Med* **13**,
718 1042-1049 (2007).
719 17. Dubois, C.*, et al.* High plasma level of S100A8/S100A9 and S100A12 at
720 admission indicates a higher risk of death in septic shock patients. *Sci Rep* **9**,
721 15660 (2019).
722 18. Clark, S.R.*, et al.* Platelet TLR4 activates neutrophil extracellular traps to
723 ensnare bacteria in septic blood. *Nat Med* **13**, 463-469 (2007).
724 19. Gao, S., Yang, Y., Fu, Y., Guo, W. & Liu, G. Diagnostic and prognostic value
725 of myeloid-related protein complex 8/14 for sepsis. *Am J Emerg Med* **33**,
726 1278-1282 (2015).
727 20. Boyd, J.H., Kan, B., Roberts, H., Wang, Y. & Walley, K.R. S100A8 and
728 S100A9 mediate endotoxin-induced cardiomyocyte dysfunction via the
729 receptor for advanced glycation end products. *Circ Res* **102**, 1239-1246
730 (2008).
731 21. Wang, Y.*, et al.* Platelet-derived S100 family member myeloid-related
732 protein-14 regulates thrombosis. *J Clin Invest* **124**, 2160-2171 (2014).
733 22. Bjork, P.*, et al.* Identification of human S100A9 as a novel target for treatment
734 of autoimmune disease via binding to quinoline-3-carboxamides. *PLoS Biol* **7**,

735 e97 (2009).

736 23. Muzumdar, M.D., Tasic, B., Miyamichi, K., Li, L. & Luo, L. A global
737 double-fluorescent Cre reporter mouse. *Genesis* **45**, 593-605 (2007).

738 24. Wu, X.*, et al.* Nicotine promotes atherosclerosis via ROS-NLRP3-mediated
739 endothelial cell pyroptosis. *Cell Death Dis* **9**, 171 (2018).

740 25. Claushuis, T.A.*, et al.* Thrombocytopenia is associated with a dysregulated
741 host response in critically ill sepsis patients. *Blood* **127**, 3062-3072 (2016).

742 26. Plunkett, A. & Tong, J. Sepsis in children. *BMJ* **350**, h3017 (2015).

743 27. Zhaolin, Z., Guohua, L., Shiyuan, W. & Zuo, W. Role of pyroptosis in
744 cardiovascular disease. *Cell Prolif* **52**, e12563 (2019).

745 28. Carestia, A., Davis, R.P., Davis, L. & Jenne, C.N. Inhibition of
746 immunothrombosis does not affect pathogen capture and does not promote
747 bacterial dissemination in a mouse model of sepsis. *Platelets* **31**, 925-931
748 (2020).

749 29. Rolfes, V.*, et al.* Platelets Fuel the Inflammasome Activation of Innate
750 Immune Cells. *Cell Rep* **31**, 107615 (2020).

751 30. Guo, Q.*, et al.* Induction of alarmin S100A8/A9 mediates activation of
752 aberrant neutrophils in the pathogenesis of COVID-19. *Cell Host Microbe* **29**,
753 222-235 e224 (2021).

754 31. Dubois, C.*, et al.* Top-Down and Bottom-Up Proteomics of Circulating
755 S100A8/S100A9 in Plasma of Septic Shock Patients. *J Proteome Res* **19**,
756 914-925 (2020).

757 32. Pirr, S.*, et al.* S100A8/A9 is the first predictive marker for neonatal sepsis.
758 *Clin Transl Med* **11**, e338 (2021).

759 33. Hottz, E.D.*, et al.* Platelets mediate increased endothelium permeability in
760 dengue through NLRP3-inflammasome activation. *Blood* **122**, 3405-3414
761 (2013).

762 34. Assinger, A., Schrottmaier, W.C., Salzmann, M. & Rayes, J. Platelets in Sepsis:

An Update on Experimental Models and Clinical Data. *Front Immunol* **10**, 1687 (2019).

35. Xu, D.F.*, et al.* Elevated angiotensin II induces platelet apoptosis through promoting oxidative stress in an AT1R-dependent manner during sepsis. *J Cell Mol Med* **25**, 4124-4135 (2021).

36. Carestia, A., Kaufman, T. & Schattner, M. Platelets: New Bricks in the Building of Neutrophil Extracellular Traps. *Front Immunol* **7**, 271 (2016).

37. Jiao, Y.*, et al.* Platelet-derived exosomes promote neutrophil extracellular trap formation during septic shock. *Crit Care* **24**, 380 (2020).

38. Chen, Z.*, et al.* Review: The Emerging Role of Neutrophil Extracellular Traps in Sepsis and Sepsis-Associated Thrombosis. *Front Cell Infect Microbiol* **11**, 653228 (2021).

39. Cecconi, M., Evans, L., Levy, M. & Rhodes, A. Sepsis and septic shock. *Lancet* **392**, 75-87 (2018).

40. Boros, F. & Vecsei, L. Progress in the development of kynurenine and quinoline-3-carboxamide-derived drugs. *Expert Opin Investig Drugs* **29**, 1223-1247 (2020).

41. Bengtsson, A.A.*, et al.* Pharmacokinetics, tolerability, and preliminary efficacy of paquinimod (ABR-215757), a new quinoline-3-carboxamide derivative: studies in lupus-prone mice and a multicenter, randomized, double-blind, placebo-controlled, repeat-dose, dose-ranging study in patients with systemic lupus erythematosus. *Arthritis Rheum* **64**, 1579-1588 (2012).

42. Liao, Y.L.*, et al.* S100A9 Upregulation Contributes to Learning and Memory Impairments by Promoting Microglia M1 Polarization in Sepsis Survivor Mice. *Inflammation* **44**, 307-320 (2021).

43. de Castro, R.E.V., Medeiros, D.N.M., Prata-Barbosa, A. & de Magalhaes-Barbosa, M.C. Surviving Sepsis Campaign International Guidelines for the Management of Septic Shock and Sepsis-Associated Organ Dysfunction in Children. *Pediatr Crit Care Med* **21**, 924-925 (2020).

792 44. Tang, W.H., *et al.* Aldose reductase-mediated phosphorylation of p53 leads to
793 mitochondrial dysfunction and damage in diabetic platelets. *Circulation* **129**,
794 1598-1609 (2014).
795 45. Dejager, L., Pinheiro, I., Dejonckheere, E. & Libert, C. Cecal ligation and
796 puncture: the gold standard model for polymicrobial sepsis? *Trends Microbiol*
797 **19**, 198-208 (2011).
798 46. Zhang, Y., *et al.* Reduced Platelet miR-223 Induction in Kawasaki Disease
799 Leads to Severe Coronary Artery Pathology Through a miR-223/PDGFRbeta
800 Vascular Smooth Muscle Cell Axis. *Circ Res* **127**, 855-873 (2020).
801 47. Angelou, A., *et al.* Platelet Depletion/Transfusion as a Lethal Factor in a
802 Colitis-associated Cancer Mouse Model. *Anticancer Res* **39**, 2443-2446
803 (2019).
804 48. Salzmann, M., *et al.* Genetic platelet depletion is superior in platelet
805 transfusion compared to current models. *Haematologica* **105**, 1738-1749
806 (2020).
807 49. Xu, M., *et al.* GPIbalpha is required for platelet-mediated hepatic
808 thrombopoietin generation. *Blood* **132**, 622-634 (2018).
809 50. de Stoppelaar, S.F., *et al.* Thrombocytopenia impairs host defense in
810 gram-negative pneumonia-derived sepsis in mice. *Blood* **124**, 3781-3790
811 (2014).
812 51. Negrotto, S., *et al.* Aspirin and salicylate suppress polymorphonuclear
813 apoptosis delay mediated by proinflammatory stimuli. *J Pharmacol Exp Ther*
814 **319**, 972-979 (2006).
815 52. Carestia, A., *et al.* Mediators and molecular pathways involved in the
816 regulation of neutrophil extracellular trap formation mediated by activated
817 platelets. *J Leukoc Biol* **99**, 153-162 (2016).
818 53. Middleton, E.A., *et al.* Neutrophil extracellular traps contribute to
819 immunothrombosis in COVID-19 acute respiratory distress syndrome. *Blood*
820 **136**, 1169-1179 (2020).

Table 1: Demographic characteristics and laboratory findings of the cohort on admission.

Variable	Total (n = 93)	Sepsis (n = 37)	Severe sepsis		P value			
			Severe (n = 22)	Shock (n = 34)	Overall	Severe vs Sepsis	Shock vs Sepsis	Shock vs Severe
Demographics								
Age < 1 year	50 (54)	20 (54)	16 (73)	14 (41)	0.0689	-	-	-
Age 1-5 years	32 (34)	16 (43)	4 (18)	12 (35)	0.1453	-	-	-
Age 5-12 years	9 (10)	1 (3)	1 (5)	7 (21)	0.0349	1.000	0.0721	0.1948
Age 12- 18 years	2 (2)	0 (0)	1 (5)	1 (3)	0.4691	-	-	-
Gender male, n (%)	53 (57)	25 (68)	12 (55)	16 (47)	0.2111	-	-	-
Medications								
Cephalosporin antibiotics, n (%)	32 (34)	17 (46)	7 (32)	8 (24)	0.1333	-	-	-
Vancomycin antibiotics, n (%)	16 (17)	1 (3)	4 (18)	11 (32)	0.0017	00593	0.0010	0.3562
Penicillin antibiotics, n (%)	15 (16)	6 (16)	5 (23)	4 (12)	0.5567	-	-	-
Typical Symptoms								
Fever, n (%)	80 (86)	36 (97)	17 (68)	27 (79)	0.01916	0.036	0.036	>0.9999
Dyspnea, n (%)	56 (60)	0 (0)	22 (100)	34 (100)	<0.0001	<0.0001	-<0.0001	>0.9999
Primary source of infection, n (%)								
Respiratory tract	61 (66)	12 (32)	22 (100)	27 (79)	<0.0001	<0.0001	0.0003	0.0627
Abdomen	14 (15)	9 (24)	2 (9)	3 (9)	0.1556	-	-	-
Skin	14 (15)	7 (19)	0 (0)	7 (21)	0.0528	-	-	-
Cardiovascular	10 (11)	3 (8)	0 (0)	7 (21)	0.0366	0.2864	0.2670	0.1046
Urinary tract	7 (8)	5 (14)	0 (0)	2 (6)	0.1804	-	-	-
Hematologic and inflammatory data								

WBC (10^9/L)	15.04 ± 11.07	19.87 ± 11.72	12.59 ± 9.81	11.25 ± 9.20	0.0023	0.0383	0.0034	>0.9999
Lymphocyte (10^9/L)	3.82 ± 4.62	5.19 ± 5.99	3.53 ± 3.45	2.47± 2.91	0.0004	0.1228	0.0003	0.4718
PMNs (10^9/L)	8.91 ± 8.00	12.51 ± 8.54	7.06 ± 8.12	6.12 ± 5.59	0.0009	0.0113	0.0023	>0.9999
Monocyte (10^9/L)	1.41 ± 1.31	1.88 ± 1.41	1.15 ± 0.81	1.05 ± 1.34	0.0004	0.0904	0.0002	0.5715
Eosinophil (10^9/L)	0.24 ± 0.68	0.16 ± 0.25	0.58 ± 1.28	0.11 ± 0.24	0.0036	0.9984	0.0364	0.0053
Basophil (10^9/L)	0.04 ± 0.10	0.04 ± 0.04	0.04 ± 0.05	0.03 ± 0.06	0.0139	>0.9999	0.0571	0.0255
N (%)	52.99 ± 19.75	55.73 ± 17.76	50.18 ± 20.97	51.82 ± 21.17	0.3938	-	-	-
L (%)	28.23 ± 18.09	27.38 ± 14.47	31.36 ± 19.15	27.12 ± 21.02	0.4530	-	-	-
RBC (10^9/L)	3.59 ± 0.81	3.98 ± 0.64	3.51 ± 0.79	3.20 ± 0.80	0.0001	0.0546	<0.0001	0.2881
HGB (g/L)	102.59 ± 26.02	111.22 ± 19.98	107.14 ± 28.29	90.26 ± 26.25	0.0003	>0.9999	0.0003	0.0210
PCT (ng/L)	21.12 ± 32.74	2.71 ± 4.62	22.35 ± 35.86	35.85 ± 36.92	<0.0001	0.0166	<0.0001	0.2702
CRP (mg/L)	81.02 ± 78.02	93.92 ± 71.90	48.3 ± 65.90	92.68 ± 88.91	0.0396	0.0485	>0.9999	0.0994
hsCRP (mg/L)	88.95 ± 83.63	47.79 ± 34.12	63.47 ± 96.30	78.11 ± 72.75	0.0124	0.0098	>0.9999	0.1150
APTT (S)	50.41 ± 14.54	43.94 ± 8.94	53.60 ± 18.21	55.20 ± 14.54	0.0006	0.0432	0.0006	>0.9999
PT (S	17.73 ± 5.12	14.64 ± 1.59	18.32 ± 5.45	20.61 ± 5.62	<0.0001	0.0011	<0.0001	0.2702
FIB (g/L)	3.79 ± 2.25	5.48 ± 2.03	2.63 ± 1.78	2.76 ± 1.59	<0.0001	<0.0001	<0.0001	0.2702
ALT (U/L)	99.22 ± 329.72	22.05 ± 18.13	31.14 ± 27.79	227.24 ± 524.96	0.0004	>0.9999	0.0005	0.0158
AST (U/L)	103.06 ± 146.28	37.05 ± 23.21	87.09 ± 79.47	185.24 ± 207.45	0.0021	0.0515	0.0025	>0.9999
LDH (U/L)	566.17 ± 703.68	256.43 ± 166.42	644.41 ± 644.76	861.30 ± 948.26	<0.0001	0.0006	<0.0001	>0.9999
ALB (g/L)	33.76 ± 7.41	37.59 ± 6.06	31.04 ± 5.24	31.36 ± 8.27	0.0001	0.0016	0.0006	0.9838
LAC (mmol/L)	3.00 ± 2.88	2.45 ±1.42	2.11 ± 1.33	4.11 ± 4.11	0.221	-	-	-
D-dimer (mg/L)	7.31 ± 6.16	1.11 ± 0.84	7.14 ± 4.55	8.49 ± 6.42	0.0006	0.0246	0.0004	>0.9999
Severity of disese								
APACHE IV score	89.69 ± 34.62	59.29 ± 20.79	79.36 ± 37.47	105.15 ± 22.04	<0.0001	<0.0001	<0.0001	>0.9999
Hospital mortality assessment (%)	35.55 ± 28.07	10.74 ± 10.20	28.60 ± 29.97	46.13 ± 20.18	<0.0001	<0.0001	<0.0001	0.8134
Mechanical ventilation (%)	57 (61)	1 (3)	22 (100)	34 (100)	<0.0001	<0.0001	<0.0001	>0.9999

Data are expressed as n/N (%) or mean ± SD unless otherwise stated. For variables with overall p values greater than 0.05, we did not perform group comparisons. Categorical variables were analyzed using Chi-square test or Fisher's exact test. One-way ANOVA and Tukey's multiple comparisons test for RBC and ALB. Kruskall-Wallis test and Dunn's multiple comparisons test for WBC, N, L, HGB, ALT, AST, LDH, LAC, D-dimer and APACHE IV score. $^{*}p < 0.05$, $^{**}p < 0.01$ and $^{***}p < 0.001$ vs. Sepsis group; $^{\#\#}p < 0.01$ vs. Severe sepsis without septic shock group. Abbreviations: WBC, white blood cell; RBC, red blood cell; PMNs, polymorphonuclear PMNs; N%, PMN to white blood cell ratio; L%, lymphocyte to white blood cell ratio; CRP, C-reactivated protein; hsCRP, high-sensitivity C-reactive protein; PCT, procalcitonin; APTT, activated partial thromboplastin time; PT, prothrombin time; FIB, fibrinogen; HGB, hemoglobin; ALT, alanine transaminase; AST; aspartate aminotransferase; LDH, lactic dehydrogenase; ALB, albumin; LAC, lactate; APACHE, acute physiology and chronic health evaluation.

Figures and Legends

Fig.1: Cohort characteristics and proteomic analysis of platelets from septic patients.

a, Pie charts showing mortality and complication in HS and septic groups (HS: n = 75, Sepsis: n = 37, Severe sepsis without septic shock: n = 22, Septic shock: n = 34). **b,** Boxplots showing the levels of IL-1β, TNFα and IL-6 in the plasma from HS and septic patients by ELISA (HS: n = 53, Sepsis: n = 15, Severe sepsis without septic shock: n = 17, Septic shock: n = 17). The boxes indicate the 25% quantile, median, and 75% quantile. **c,** Violin plots showing the platelet parameters MPV (HS: n = 75, Sepsis: n = 37, Severe sepsis without septic shock: n = 21, Septic shock: n = 31), PDW (HS: n = 73, Sepsis: n = 37, Severe sepsis without septic shock: n = 21, Septic shock: n = 30) and P-LCR (HS: n = 75, Sepsis: n = 37, Severe sepsis without septic shock: n = 21, Septic shock: n = 31)) among septic groups. **d,** Scatterplots showing platelet counts of sepsis, severe sepsis without septic shock and septic shock patients along the time (28 days) axis (Sepsis: n = 37, Severe sepsis without septic shock: n = 21, Septic shock: n = 30). **e,** Schematic diagram of the experimental design for DIA-MS (HS: n = 3, Severe sepsis: n = 3). Volcano plot with significantly increased (red) and decreased (blue) expression of proteins from HS and septic groups. Fold change cutoff > 1.5 and p value < 0.05. **f,** Bar plots of the enriched GO biological processes, KEGG or Reactome terms of highly expressed genes from septic groups. **g,** Heatmap of representative proteins related to different cell deaths signal pathways in severe sepsis and HS samples. **h,** Bar graphs displaying the percentage of activations

of caspase 3/7 (HS: n = 27, Severe sepsis: n = 27), LC3B (HS: n = 15, Severe sepsis: n = 15), and caspase 1 (HS: n = 27, Severe sepsis: n = 27) in septic and HS platelets using FACS. The boxes indicate the 25% quantile, median, and 75% quantile. Data was presented as mean ± SD or median with interquartile range. Kruskall-Wallis test and Dunn's multiple comparisons test for **b, c**. Mann Whitney test for **h**. $^{*}p < 0.05$, $^{**}p < 0.01$ and $^{***}p < 0.001$ vs. HS group; $^{\#}p < 0.05$, $^{\#\#}p < 0.01$ and $^{\#\#\#}p < 0.001$ vs. Sepsis group. Abbreviation is as follow: HS, healthy subjects; y, year-old; MPV, mean platelet volume; PDW, platelet distribution width; P-LCR, platelet large cell ratio; PLT, platelet; NS, not statistically significant; Severe sepsis, severe sepsis/septic shock.

Fig.2: GSDMD-dependent pyroptosis ensues in septic platelets.

a, Representative low and high power TEM fields showing platelet ultrastructures from severe sepsis patients and HS (HS: n = 5, Severe sepsis: n = 5). Red arrowheads indicate swelling and rupture of the platelet plasma membrane during severe sepsis. The magnified TEM showed a swollen platelet that had ruptured (region around red arrow) and release of its cellular contents. Scale bars: 1 μm and 500 nm. **b,** Immunofluorescence analysis showing the co-localization of CD41 (green), ASC (red) and NLRP3 (blue) in platelets from severe sepsis (HS: n = 8, Severe sepsis: n = 8). Purple indicates overlap. Scale bars: 5 μm and 1 μm. The quantified results are shown on the right. **c,** The expression and quantification of pro-caspase 1 and activated caspase 1 in platelets from severe sepsis were determined by western blot (HS: n = 6, Severe sepsis: n = 6). **d,** The expression and quantification of GSDMD and GSDMD

N-terminus proteins in platelets from severe sepsis were detected using western blot (HS: n = 6, Severe sepsis: n = 6). **e,** FACS analysis of the activated caspase 1 in platelets from severe sepsis (HS: n = 13, Severe sepsis: n = 23). The quantified results are shown on the right. **f,** Expression of IL-1β in platelets from HS and septic groups (HS: n = 8, Severe sepsis: n = 8). **g,** Live-imaging of platelets from *Gsdmd*$^{fl/fl}$ PF4-Cre mice and *Gsdmd*$^{fl/fl}$ mice induced by LPS (10 μg/ml) and Nigericin (5 μM) for 20 minutes (n = 6); Scale bars: 10 μm. **h,** Representative TEM field of platelets from the *Gsdmd*$^{fl/fl}$ PF4-Cre mice and *Gsdmd*$^{fl/fl}$ mice with or without CLP operation (n = 5). Scale bars: 1 μm. Data was presented as mean ± SD or median with interquartile range. Unpaired t test for **b-g**. Kruskall-Wallis test and Dunn's multiple comparisons test for **h**. $^{*}p < 0.05$, $^{**}p < 0.01$ and $^{***}p < 0.001$. Abbreviation is as follow: HS, healthy subjects; Severe sepsis, severe sepsis/septic shock; NS, not statistically significant.

Fig.3: S100A8/A9 induces platelet pyroptosis through TLR4 pathway.

a, Scatterplot displaying correlation of platelet pyroptosis (activated caspase 1 positive platelets) with the plasma levels of S100A8/A9 in severe sepsis patients and HS (n = 49, r, correlation coefficient). **b,** Immunofluorescence analysis showing co-expression of CD41 (green), ASC (red) and NLRP3 (blue) in platelets treated with 1 μg/ml rhS100A8/A9 or 10 μM Paquinimod (n = 6); Purple indicates overlap. Scale bars: 5 μm and 1 μm. The quantified results are shown on the right. **c,** FACS analysis and bar graphs displaying the caspase 1 activity of platelets treated with 1 μg/ml rhS100A8/A9 or 10 μM Paquinimod (n = 6). **d,** The expression and quantification of

GSDMD and GSDMD N-terminus in platelets treated with 1 μg/ml rhS100A8/A9 or 10 μM Paquinimod were determined using western blot (n = 6). **e, f,** In LPS induced murine model, mice depleted of platelets were transfused with a total of 1.2 x 10^7 purified platelets (volume: 200 μl, concentration: 6 x 10^{10} platelets/L) from *Tlr4*$^{-/-}$ or WT mice (n = 6). Bar graphs displaying the percentage of NLRP3-ASC inflammasome **(e)** in platelets using immunofluorescence assays and caspase 1 activity **(f)** in platelets by FACS analysis. **g,** Boxplots displaying abundant mitochondrial ROS production in platelets from severe sepsis using FACS analysis (HS: n = 18, Severe sepsis: n = 19). The boxes indicate the 25% quantile, median, and 75% quantile. **h,** Bar graphs displaying the caspase 1 activity in septic platelets treated with 5 mM MitoTempo or PBS by FACS analysis (n = 6). **i,** Bar graphs displaying the mitochondrial ROS production in platelets treated with 1 μg/ml rhS100A8/A9 and 10 μM Paquinimod using FACS analysis (n = 6). Data was presented as mean (or fluorescence) ± SD. Pearson's correlation test for **a**. Mann Whitney test for **g**. One-way ANOVA and Tukey's multiple comparisons test for (**b-f, h** and **i**). $^{*}p < 0.05$, $^{**}p < 0.01$ and $^{***}p < 0.001$. Abbreviation is as follow: Vehicle control, platelets from HS treated with HBSS; rhS100A8/A9, platelets from HS treated with rhS100A8/A9; rhS100A8/A9+Paq, platelets from HS treated with rhS100A8/A9 and Paquinimod; PBS, PBS-injected mice; LPS+saline, LPS-injected mice transfused with normal saline; LPS+WT PLTs, LPS-injected mice transfused with WT platelets; LPS+*Tlr4*$^{-/-}$ PLTs, LPS-injected mice transfused with *Tlr4*$^{-/-}$ platelets; HS, healthy subjects; Severe sepsis, severe sepsis/septic shock; NS, not statistically significant.

Fig.4: Pyroptotic platelets promote NET formation via releasing ox-mtDNA.

a, Boxplots showing quantification of MPO-DNA and dsDNA (NET structures) in the plasma of HS and severe sepsis patients using PicoGreen fluorescent dye and MPO-DNA-ELISA, respectively (HS: n = 53, Severe sepsis: n = 51). The boxes indicate the 25% quantile, median, and 75% quantile. **b**, Scatterplots displaying correlations of platelet pyroptosis (activated caspase 1 positive platelets) with the levels of MPO-DNA complexes and dsDNA in plasma of severe sepsis patients and HS (r, correlation coefficient; n = 49). **c**, Immunofluorescence analysis showing either 50 nM PMA or 1 μg/ml S100A8/A9-induced pyroptotic platelets induced NET formation. Cells were stained with Hoechst for DNA (blue), anti-MPO for PMNs or NETs (green), CD41 for platelet (red); scale bars: 25 μm and 7.5 μm. **d**, Quantification of MPO-DNA and dsDNA in the supernatant of cells using PicoGreen fluorescent dye and MPO-DNA-ELISA, respectively (n = 6). **e**, Immunofluorescence analysis showing NET formation in PMNs treated with rmS100A8/A9-induced platelets (WT or *Tlr4*$^{-/-}$) (n = 6). Cells were stained with Hoechst for DNA (blue), anti-MPO for PMNs or NETs (red), CD41 for platelet (green); Scale bars: 25 μm and 7.5 μm. **f**, Bar graphs displaying the levels of MPO-DNA and dsDNA in the supernatant of cells treated with rmS100A8/A9-induced platelets (*Tlr4*$^{-/-}$ or WT) using PicoGreen fluorescent dye and MPO-DNA-ELISA, respectively (n = 6). **g**, The levels of ox-mtDNA in supernatant of S100A8/A9-induced pyroptotic platelets (for 4 hours) were determined by General 8-OHdG ELISA Kit (n = 5). **h**, The levels of ox-mtDNA in plasma of patients and HS were determined by General 8-OHdG ELISA Kit (HS: n

= 13, Sepsis: n = 11, Severe sepsis: n = 17). **i**, The levels of ox-mtDNA in plasma of sham or CLP mice (for 6 hours) were determined by General 8-OHdG ELISA Kit (Sham: n = 7, CLP: n = 9). Data was presented as mean ± SD. Mann Whitney test for **a**. Pearson's correlation test for **b**. One-way ANOVA and Tukey's multiple comparisons test for **d**, **f** and **g**. Kruskall-Wallis test and Dunn's multiple comparisons test for **h**. Unpaired t test for **i**. $^{*}p < 0.05$, $^{**}p < 0.01$ and $^{***}p < 0.001$. Abbreviation is as follow: HS, healthy subjects; Severe sepsis, severe sepsis/septic shock; PLTs, platelets, PMNs, polymorphonuclear neutrophils; NS, not statistically significant.

Fig.5: NET formation in turn induces platelet pyroptosis via the release of S100A8/A9.

a, The S100A8/A9 released from NETs (either PMA or rhS100A8/A9-induced pyroptotic platelets induced NET formation for 4 hours) was determined by ELISA (n = 5). **b**, Representative immunofluorescence images of pyroptotic platelets incubated with PMA-treated murine PMNs (WT or *S100a9*$^{-/-}$). Cells were stained with Hoechst for DNA (blue), anti-MPO for PMNs or NETs (cyan), CD41 for platelet (red) and caspase 1 for pyroptosis (green); scale bars: 25 μm and 5 μm. **c**, Bar graphs displaying mitochondrial ROS production in platelets co-cultured with PMA-treated murine PMNs (WT or *S100a9*$^{-/-}$) using FACS analysis (n = 5). **d**, Immunofluorescence analysis showing co-expression of CD41 (green), ASC (red) and NLRP3 (blue) in platelets co-cultured with PMA-treated murine PMNs (WT or *S100a9*$^{-/-}$) (n = 5). Purple indicates overlap. Scale bars: 5 μm and 1 μm. **e**, The quantified results of NLRP3 inflammasome are shown on the below. **f**, Bar graphs displaying the caspase 1

activity of platelets co-cultured with PMA-treated murine PMNs (WT or *S100a9*$^{-/-}$) by FACS analysis (n = 5). Data was presented as mean ± SD. One-way ANOVA and Tukey's multiple comparisons test for (**a**, **c**, **e** and **f**). $^{*}p < 0.05$, $^{**}p < 0.01$ and $^{***}p < 0.001$. Abbreviation is as follow: PLTs, platelets, PMNs, polymorphonuclear neutrophils.

Fig.6: *Gsdmd* deficiency in platelets ameliorates excessive NET-mediated inflammation in sepsis mice.

a, Immunofluorescence analysis showing NET formation treated with S100A8/A9-induced platelets from *Gsdmd*$^{fl/fl}$ PF4-Cre mice and *Gsdmd*$^{fl/fl}$ mice (n = 5). Cells were stained with Hoechst for DNA (blue), anti-MPO for PMNs or NETs (red), CD41 for platelet (green). Scale bars: 25 μm and 7.5 μm. **b**, **c**, Bar graphs displaying the levels of MPO-DNA (**b**) and dsDNA (**c**) in supernatant of rmS100A8/A9-induced platelets from *Gsdmd*$^{fl/fl}$ PF4-Cre mice and *Gsdmd*$^{fl/fl}$ mice (for 4 hours) using PicoGreen fluorescent dye and MPO-DNA-ELISA, respectively (n = 5). In CLP-induced sepsis murine model, the levels of NETs and proinflammatory cytokines in plasma of mice were detected using ELISA kits after 6 hours of CLP operation. **d**, **e** Bar graphs displaying the levels of MPO-DNA complexes (**d**) and dsDNA (**e**) in plasma of *Gsdmd*$^{fl/fl}$ PF4-Cre mice and *Gsdmd*$^{fl/fl}$ mice using PicoGreen fluorescent dye and MPO-DNA-ELISA, respectively (n = 5~6). **f-h**, Bar graphs showing the levels of IL-1β (**f**), TNFα (**g**) and IL-6 (**h**) in plasma of *Gsdmd*$^{fl/fl}$ PF4-Cre mice and *Gsdmd*$^{fl/fl}$ mice by CLP (n = 4~5). **i**, Survival analysis of *Gsdmd*$^{fl/fl}$ PF4-Cre mice and *Gsdmd*$^{fl/fl}$ mice in CLP-induced sepsis model for 7 days (n = 11). Data was

presented as mean ± SD. One-way ANOVA and Tukey's multiple comparisons test for **b-h**. Log-rank (Mantel-Cox) test for **i**. $^{*}p < 0.05$, $^{**}p < 0.01$ and $^{***}p < 0.001$. Abbreviation is as follow: PLTs, platelets; PMNs, polymorphonuclear neutrophils; NS, not statistically significant.

Fig.7: Paquinimod ameliorates NET-mediated inflammation and improves survival rate by suppressing platelet pyroptosis.

In the CLP-induced sepsis model, mice that were given Paquinimod (10 mg/kg/day) or PBS by oral gavage for 5 days (n = 6 mice/group). **a**, Bar graphs showing the plasma levels of heterodimer S100A8/A9 in mice. **b**, **c**, Bar graphs showing mitochondrial ROS production (**b**) and caspase 1 activity (**c**) in murine platelets using FACS analysis. **d**, **e**, Quantification of MPO-DNA (**d**) and dsDNA (**e**) in the plasma of mice was assessed using PicoGreen fluorescent dye and MPO-DNA ELISA kit, respectively. **f-h**, Bar graphs displaying the levels of IL-1β (**f**), TNFα (**g**) and IL-6 (**h**) in plasma of mice. **i**, Survival analysis of CLP-induced sepsis mice treated with Paquinimod for 5 days. Data was presented as mean (or fluorescence) ± SD. One-way ANOVA and Tukey's multiple comparisons test for **a-h**. Log-rank (Mantel-Cox) test for survival curves **i**. $^{*}p < 0.05$, $^{**}p < 0.01$ and $^{***}p < 0.001$. Abbreviation is as follow: Sham, sham-operated mice, CLP-induced sepsis mice with PBS; CLP+Paq, CLP-induced sepsis mice with Paquinimod; NS, not statistically significant.

Fig.8: GSDMD-dependent platelet pyroptosis exacerbates NET formation and inflammation in severe sepsis.

Sepsis-derived S100A8/A9 induces GSDMD-dependent platelet pyroptosis via the TLR4/ROS/NLRP3/caspase 1/GSDMD pathway in severe sepsis. Pyroptotic platelets promote NET formation via ox-mtDNA, while NETs in turn lead to more platelet pyroptosis via release of S100A8/A9, forming a platelet pyroptosis-NET feedback loop.

Fig 1

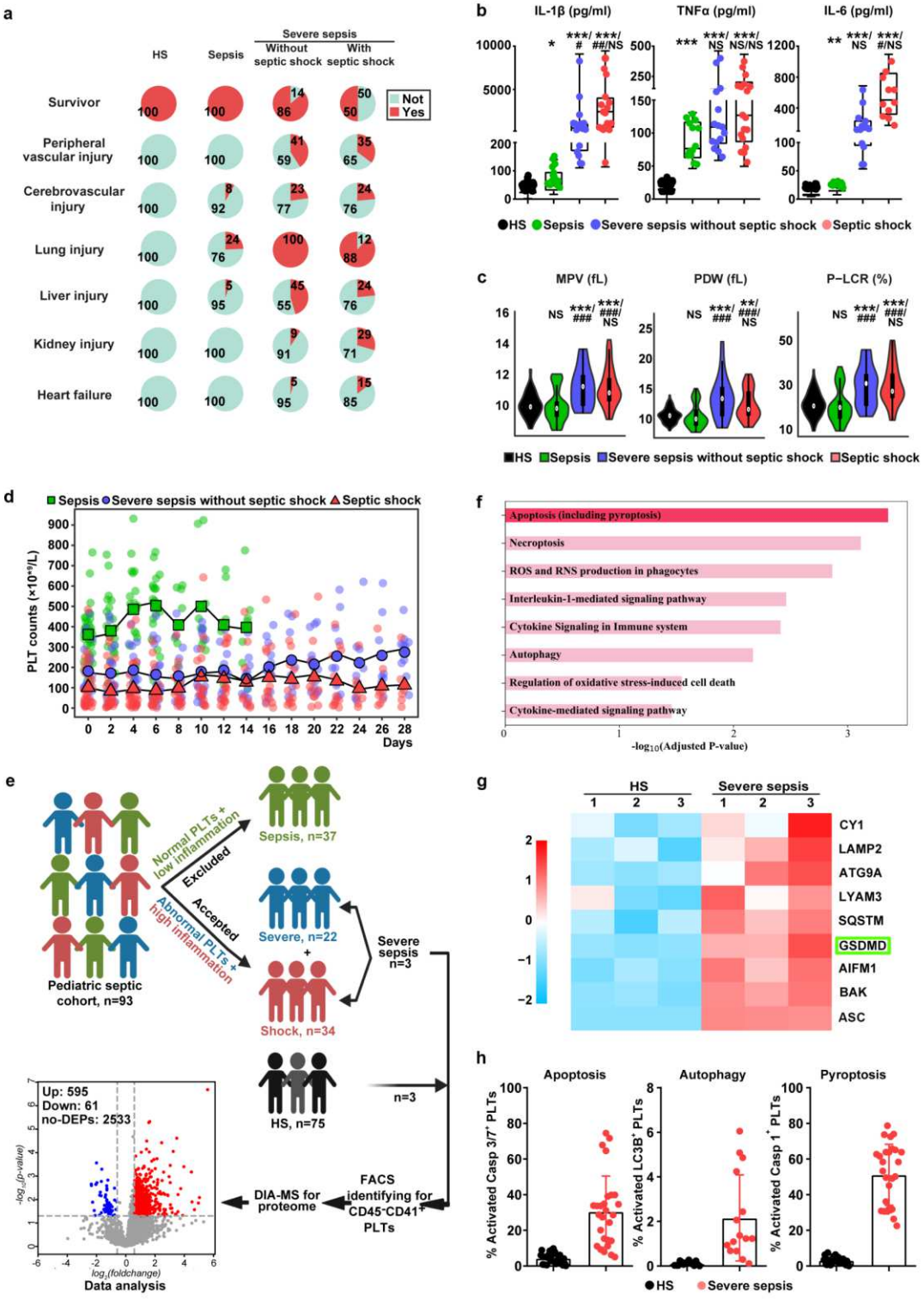
a
HS
Sepsis
Severe sepsis
Without septic shock
With septic shock
Not
Yes
Survivor
Peripheral vascular injury
Cerebrovascular injury
Lung injury
Liver injury
Kidney injury
Heart failure
b
IL-1β (pg/ml)
TNFα (pg/ml)
IL-6 (pg/ml)
HS
Sepsis
Severe sepsis without septic shock
Septic shock
c
MPV (fL)
PDW (fL)
P-LCR (%)
d
PLT counts (×10^9/L)
Days
e
Pediatric septic cohort, n=93
Normal PLTs + low inflammation
Excluded
Abnormal PLTs + high inflammation
Accepted
Sepsis, n=37
Severe, n=22
Shock, n=34
Severe sepsis n=3
HS, n=75
n=3
FACS identifying for CD45-CD41+ PLTs
DIA-MS for proteome
Up: 595
Down: 61
no-DEPs: 2533
Data analysis
f
Apoptosis (including pyroptosis)
Necroptosis
ROS and RNS production in phagocytes
Interleukin-1-mediated signaling pathway
Cytokine Signaling in Immune system
Autophagy
Regulation of oxidative stress-induced cell death
Cytokine-mediated signaling pathway
-log10(Adjusted P-value)
g
HS
Severe sepsis
CY1
LAMP2
ATG9A
LYAM3
SQSTM
GSDMD
AIFM1
BAK
ASC
h
Apoptosis
Autophagy
Pyroptosis
% Activated Casp 3/7+ PLTs
% Activated LC3B+ PLTs
% Activated Casp 1+ PLTs
HS
Severe sepsis

1017

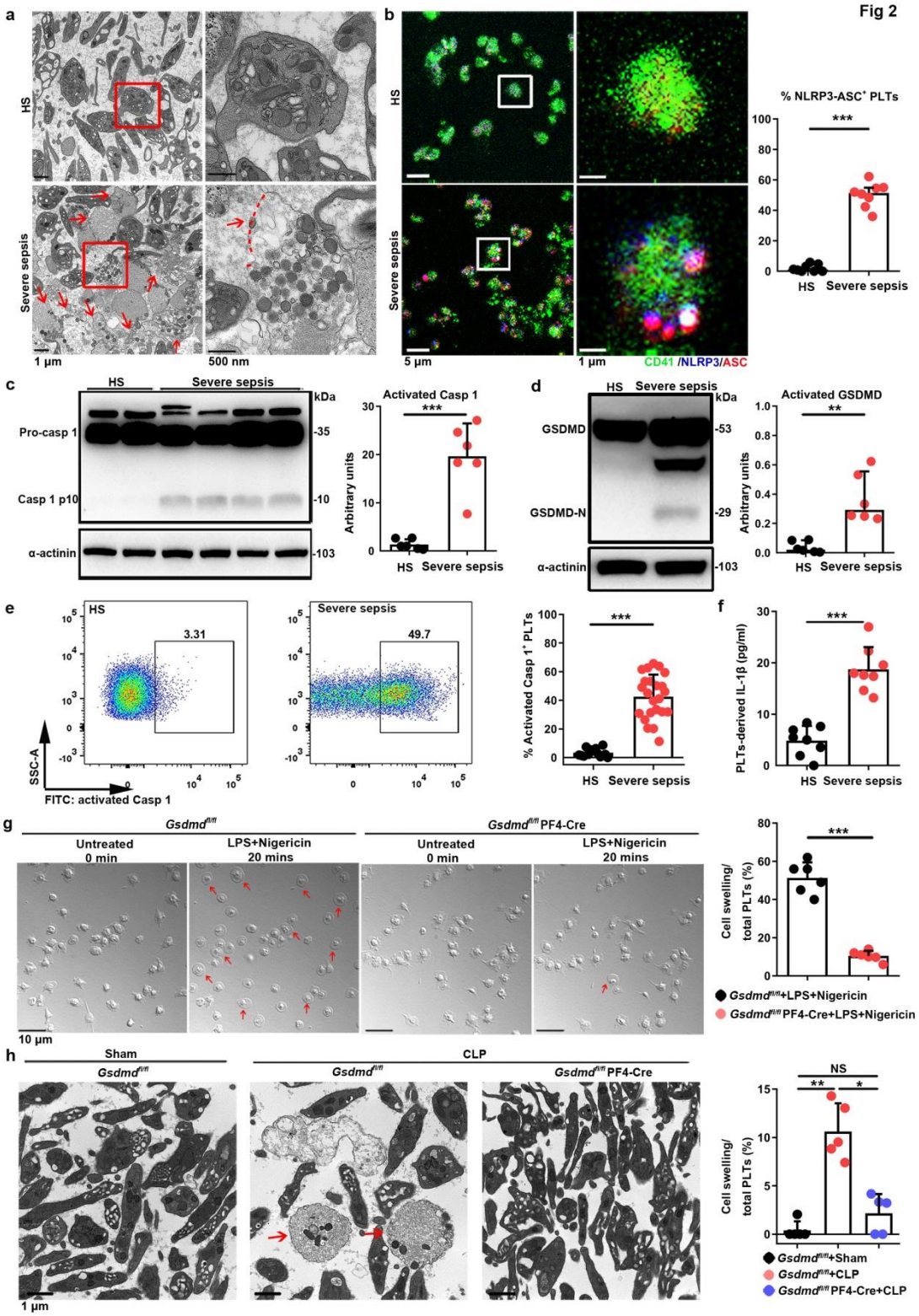
Fig 2
a
HS
Severe sepsis
1 μm
500 nm
b
HS
Severe sepsis
5 μm
1 μm
CD41 /NLRP3/ASC
% NLRP3-ASC+ PLTs
***
HS Severe sepsis
c
HS Severe sepsis
kDa
Pro-casp 1
Casp 1 p10
α-actinin
-35
-10
-103
Activated Casp 1
***
Arbitrary units
HS Severe sepsis
d
HS Severe sepsis
kDa
GSDMD
GSDMD-N
α-actinin
-53
-29
-103
Activated GSDMD
**
Arbitrary units
HS Severe sepsis
e
HS
3.31
Severe sepsis
49.7
SSC-A
FITC: activated Casp 1
% Activated Casp 1+ PLTs
***
HS Severe sepsis
f
PLTs-derived IL-1β (pg/ml)
***
HS Severe sepsis
g
Gsdmdfl/fl
Gsdmdfl/fl PF4-Cre
Untreated
0 min
LPS+Nigericin
20 mins
10 μm
Cell swelling/ total PLTs (%)
***
Gsdmdfl/fl+LPS+Nigericin
Gsdmdfl/fl PF4-Cre+LPS+Nigericin
h
Sham
CLP
Gsdmdfl/fl
Gsdmdfl/fl
Gsdmdfl/fl PF4-Cre
1 μm
NS
**
*
Cell swelling/ total PLTs (%)
Gsdmdfl/fl+Sham
Gsdmdfl/fl+CLP
Gsdmdfl/fl PF4-Cre+CLP

1018

Fig 3

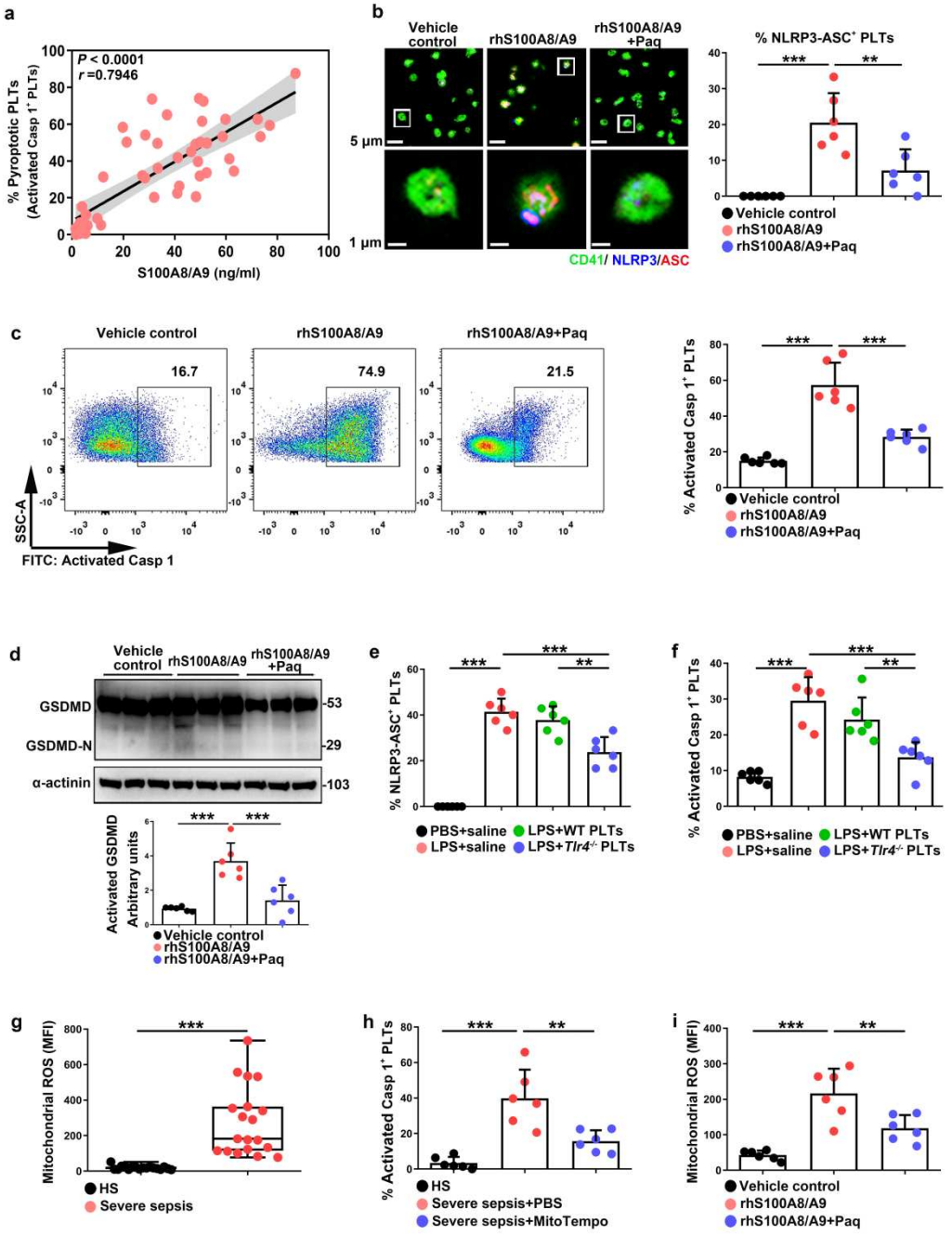
a
P < 0.0001
r =0.7946
% Pyroptotic PLTs (Activated Casp 1+ PLTs)
S100A8/A9 (ng/ml)
b
Vehicle control
rhS100A8/A9
rhS100A8/A9 +Paq
5 µm
1 µm
CD41/ NLRP3/ASC
% NLRP3-ASC+ PLTs
Vehicle control
rhS100A8/A9
rhS100A8/A9+Paq
c
Vehicle control
rhS100A8/A9
rhS100A8/A9+Paq
16.7
74.9
21.5
SSC-A
FITC: Activated Casp 1
% Activated Casp 1+ PLTs
d
GSDMD
GSDMD-N
α-actinin
53
29
103
Activated GSDMD Arbitrary units
e
% NLRP3-ASC+ PLTs
PBS+saline
LPS+saline
LPS+WT PLTs
LPS+Tlr4-/- PLTs
f
% Activated Casp 1+ PLTs
g
Mitochondrial ROS (MFI)
HS
Severe sepsis
h
% Activated Casp 1+ PLTs
Severe sepsis+PBS
Severe sepsis+MitoTempo
i
Mitochondrial ROS (MFI)

1019

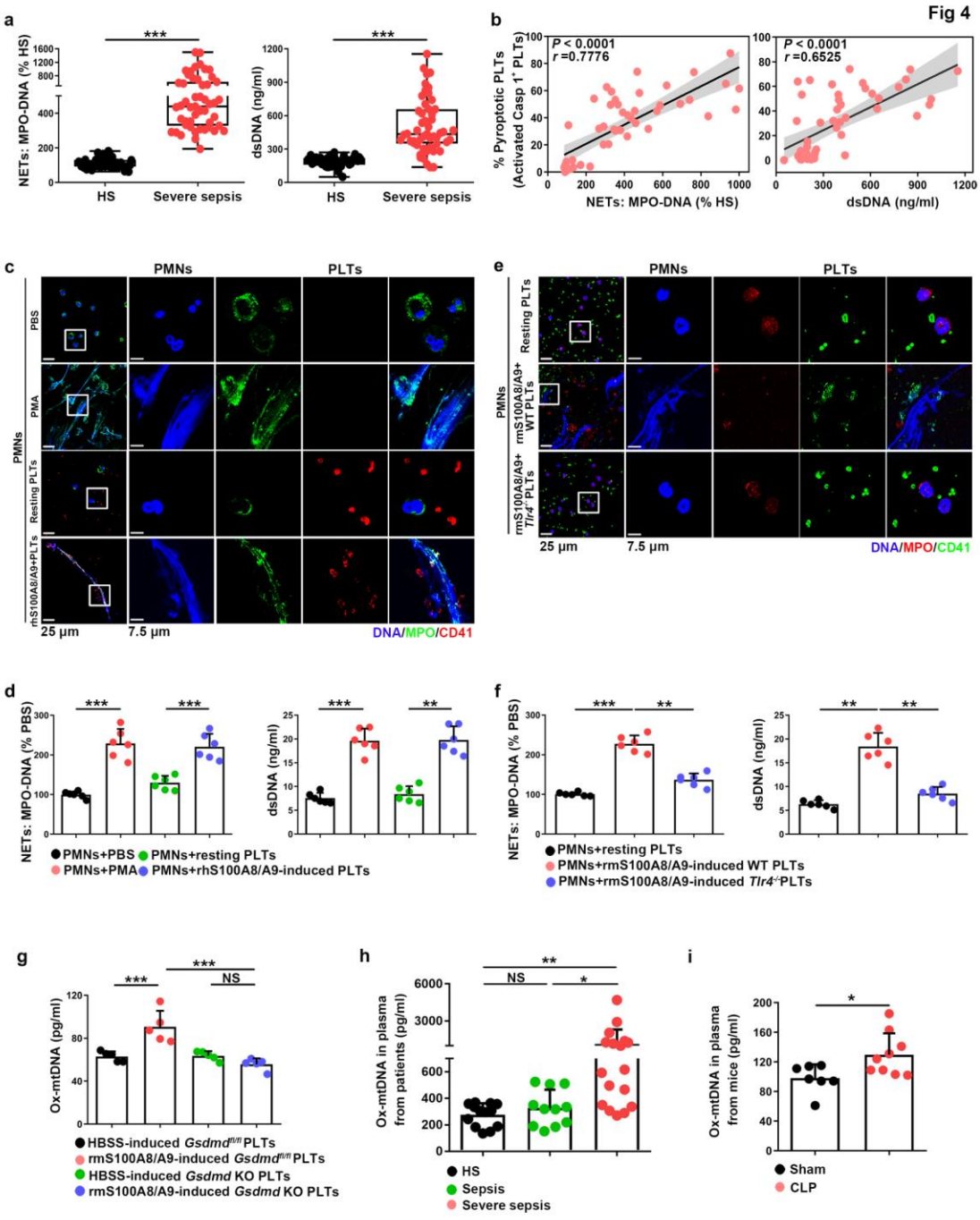
Fig 4
a
NETs: MPO-DNA (% HS)
dsDNA (ng/ml)
HS
Severe sepsis
b
% Pyroptotic PLTs (Activated Casp 1+ PLTs)
P < 0.0001
r =0.7776
P < 0.0001
r =0.6525
NETs: MPO-DNA (% HS)
dsDNA (ng/ml)
c
PMNs
PLTs
PBS
PMA
Resting PLTs
rhS100A8/A9+PLTs
25 μm
7.5 μm
DNA/MPO/CD41
e
Resting PLTs
rmS100A8/A9+ WT PLTs
rmS100A8/A9+ Tlr4-/- PLTs
d
NETs: MPO-DNA (% PBS)
dsDNA (ng/ml)
PMNs+PBS
PMNs+resting PLTs
PMNs+PMA
PMNs+rhS100A8/A9-induced PLTs
f
PMNs+rmS100A8/A9-induced WT PLTs
PMNs+rmS100A8/A9-induced Tlr4-/- PLTs
g
Ox-mtDNA (pg/ml)
NS
HBSS-induced Gsdmdfl/fl PLTs
rmS100A8/A9-induced Gsdmdfl/fl PLTs
HBSS-induced Gsdmd KO PLTs
rmS100A8/A9-induced Gsdmd KO PLTs
h
Ox-mtDNA in plasma from patients (pg/ml)
HS
Sepsis
Severe sepsis
i
Ox-mtDNA in plasma from mice (pg/ml)
Sham
CLP

1020

Fig 5

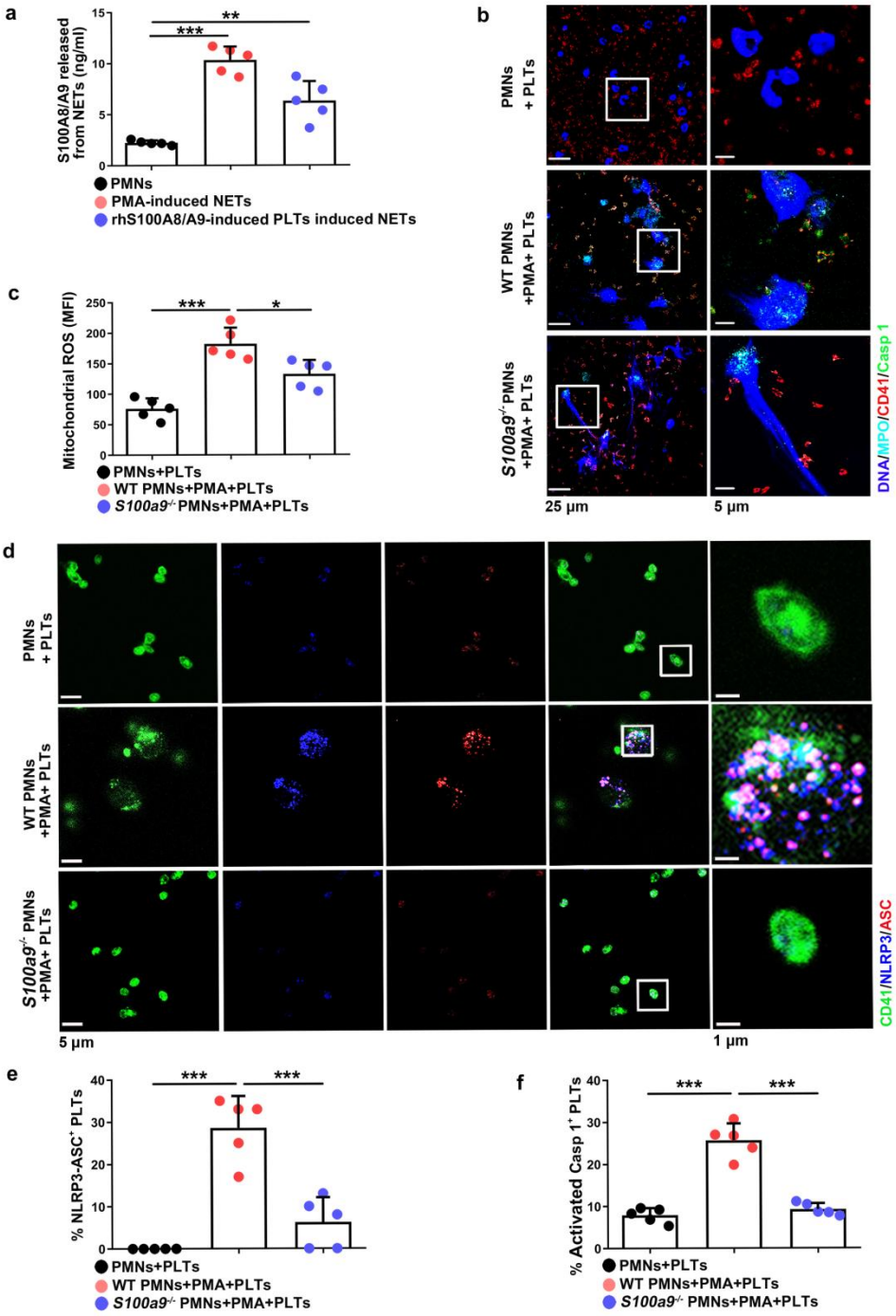
a
S100A8/A9 released from NETs (ng/ml)
**
***
PMNs
PMA-induced NETs
rhS100A8/A9-induced PLTs induced NETs
b
PMNs + PLTs
WT PMNs +PMA+ PLTs
S100a9-/- PMNs +PMA+ PLTs
DNA/MPO/CD41/Casp 1
25 µm
5 µm
c
Mitochondrial ROS (MFI)
***
*
PMNs+PLTs
WT PMNs+PMA+PLTs
S100a9-/- PMNs+PMA+PLTs
d
PMNs + PLTs
WT PMNs +PMA+ PLTs
S100a9-/- PMNs +PMA+ PLTs
CD41/NLRP3/ASC
5 µm
1 µm
e
% NLRP3-ASC+ PLTs
***
***
PMNs+PLTs
WT PMNs+PMA+PLTs
S100a9-/- PMNs+PMA+PLTs
f
% Activated Casp 1+ PLTs
***
***
PMNs+PLTs
WT PMNs+PMA+PLTs
S100a9-/- PMNs+PMA+PLTs

1021

Fig 6

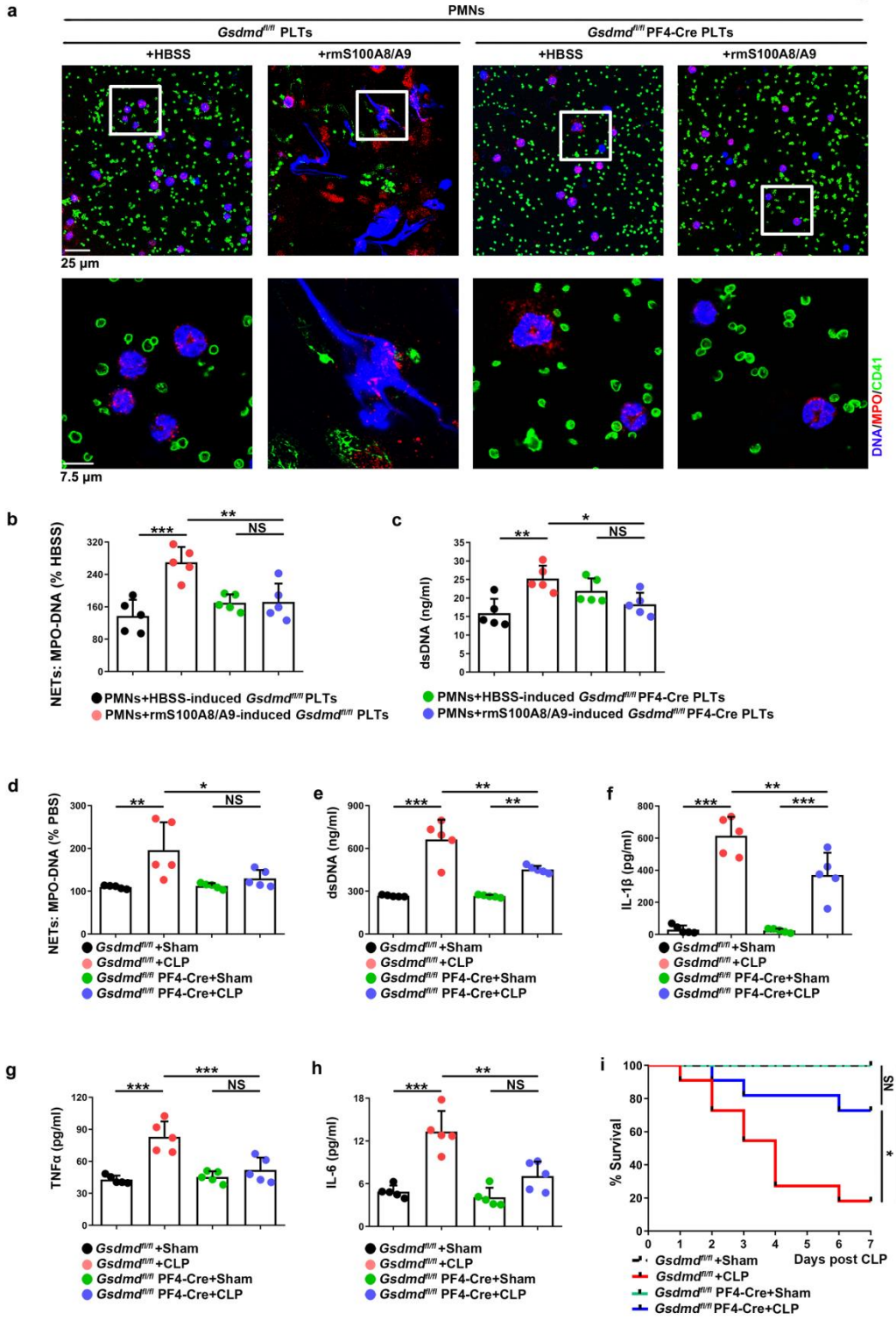
a
PMNs
Gsdmd fl/fl PLTs
Gsdmd fl/fl PF4-Cre PLTs
+HBSS
+rmS100A8/A9
+HBSS
+rmS100A8/A9
25 μm
7.5 μm
DNA/MPO/CD41
b
NETs: MPO-DNA (% HBSS)
PMNs+HBSS-induced Gsdmd fl/fl PLTs
PMNs+rmS100A8/A9-induced Gsdmd fl/fl PLTs
c
dsDNA (ng/ml)
PMNs+HBSS-induced Gsdmd fl/fl PF4-Cre PLTs
PMNs+rmS100A8/A9-induced Gsdmd fl/fl PF4-Cre PLTs
d
NETs: MPO-DNA (% PBS)
e
dsDNA (ng/ml)
f
IL-1β (pg/ml)
Gsdmd fl/fl +Sham
Gsdmd fl/fl +CLP
Gsdmd fl/fl PF4-Cre+Sham
Gsdmd fl/fl PF4-Cre+CLP
g
TNFα (pg/ml)
h
IL-6 (pg/ml)
i
% Survival
Days post CLP
NS
Gsdmd fl/fl +Sham
Gsdmd fl/fl +CLP
Gsdmd fl/fl PF4-Cre+Sham
Gsdmd fl/fl PF4-Cre+CLP

1022

Fig 7

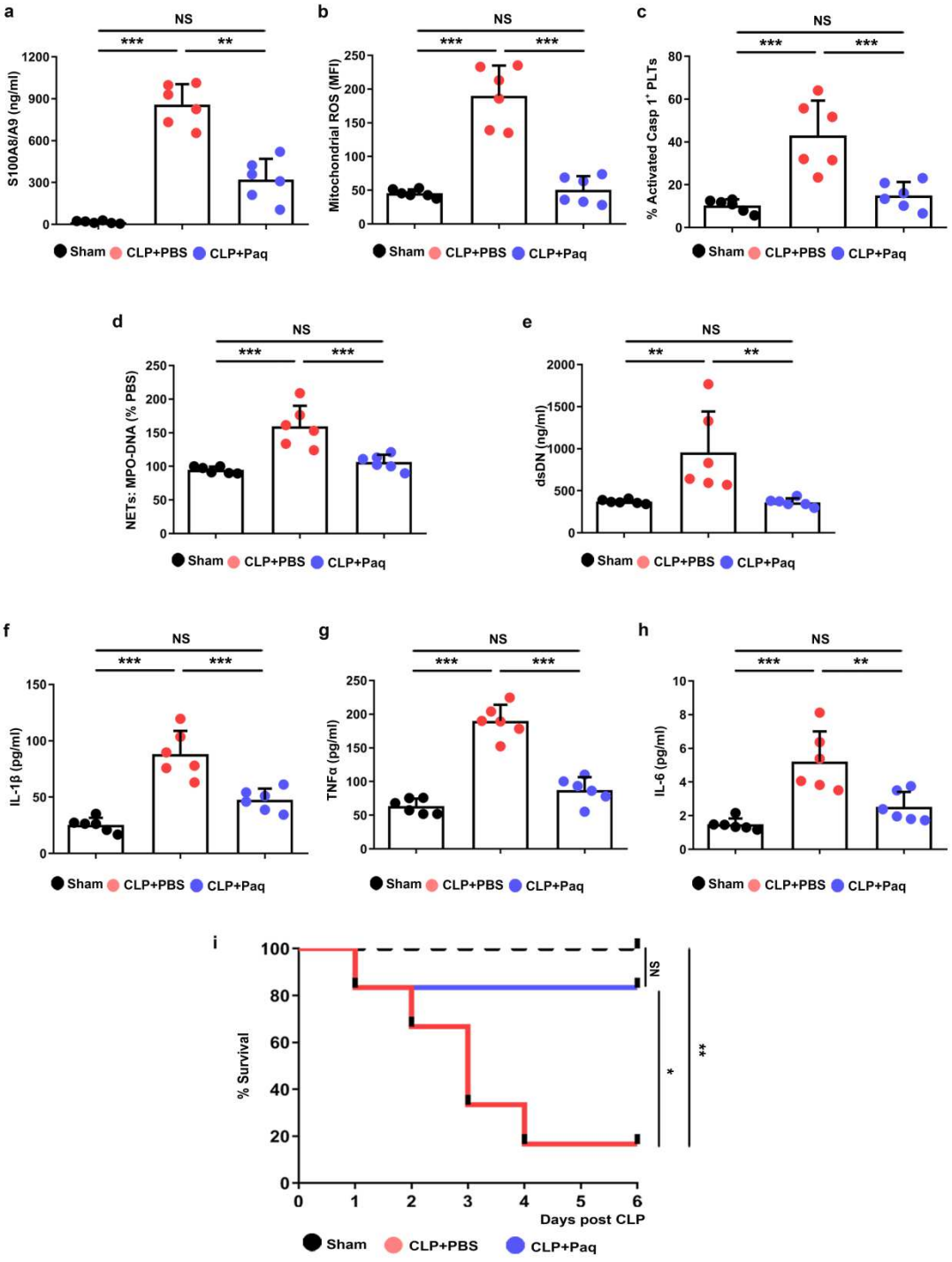
a
b
c
d
e
f
g
h
i
NS
***
**
S100A8/A9 (ng/ml)
Mitochondrial ROS (MFI)
% Activated Casp 1+ PLTs
NETs: MPO-DNA (% PBS)
dsDN (ng/ml)
IL-1β (pg/ml)
TNFα (pg/ml)
IL-6 (pg/ml)
% Survival
Days post CLP
Sham
CLP+PBS
CLP+Paq

1023

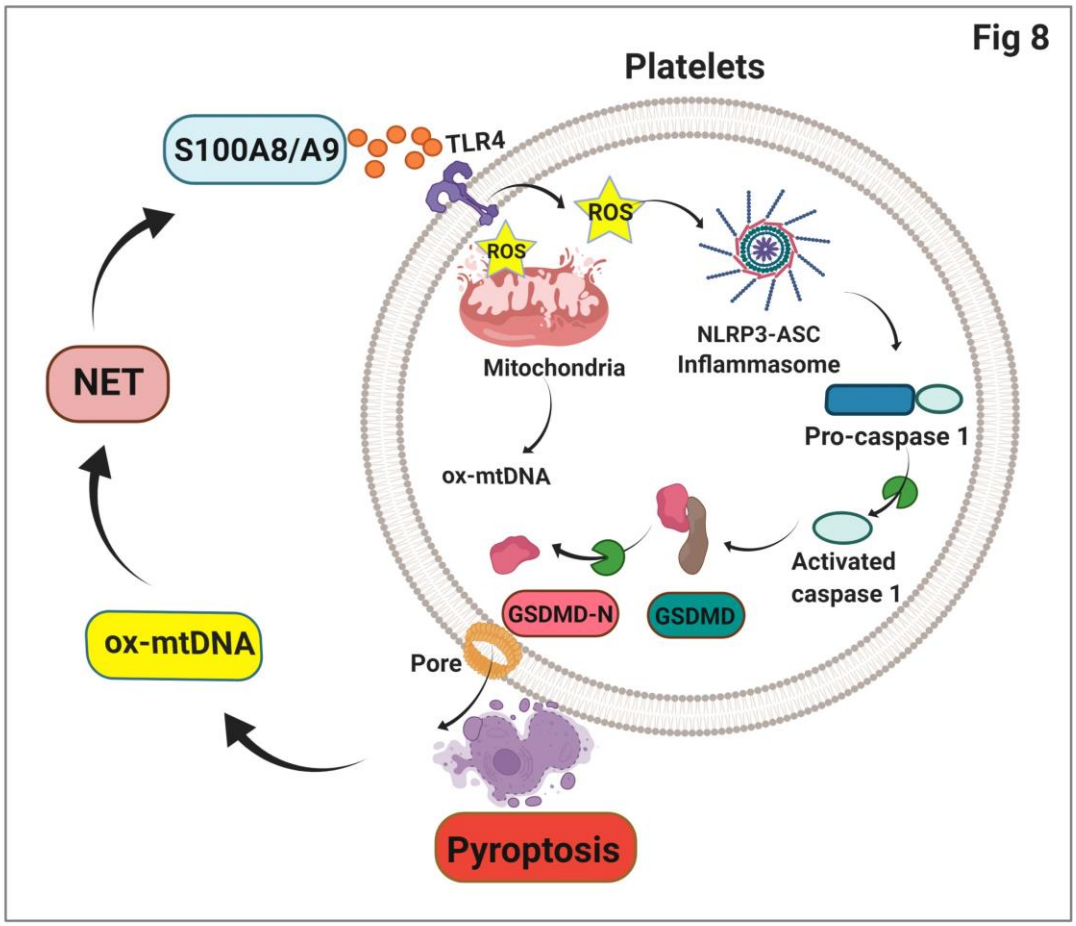
Fig 8
Platelets
S100A8/A9
TLR4
ROS
ROS
Mitochondria
NLRP3-ASC
Inflammasome
Pro-caspase 1
ox-mtDNA
Activated
caspase 1
GSDMD-N
GSDMD
Pore
NET
ox-mtDNA
Pyroptosis

1024

Supplementary Files

This is a list of supplementary files associated with this preprint. Click to download.

- SupplementaryMaterialsPyroptosisinsepsis3172022.pdf
- GsdmdfloxPLTsvideo1.avi
- GsdmdKOPLTsvideo2.avi